Synergistic reinforcement learning by cooperation of the cerebellum and basal ganglia

Tatsumi Yoshida[1]*, Hikaru Sugino[1]*, Hinako Yamamoto[1]*, Sho Tanno[1], Mikihide Tamura[1], Jun Igarashi[2], Yoshikazu Isomura[1†], Riichiro Hira[1†]

Affiliates:
1. Department of Physiology and Cell Biology, Graduate School of Medical and Dental Sciences, Tokyo Medical and Dental University, Tokyo, Japan
2. High Performance Artificial Intelligent System Research Team, Center for Computational Science, RIKEN, Saitama, Japan
* These authors equally contributed to this work.
† Corresponding authors.

Correspondence:
Riichiro Hira, M.D. Ph.D. rhira.phy2@tmd.ac.jp
Department of Physiology and Cell Biology, Graduate School of Medical and Dental Sciences, Tokyo Medical and Dental University, 1-5-45 Yushima, Bunkyo-ku, Tokyo, 113-8510, Japan.

Yoshikazu Isomura, Ph.D. isomura.phy2@tmd.ac.jp
Department of Physiology and Cell Biology, Graduate School of Medical and Dental Sciences, Tokyo Medical and Dental University, 1-5-45 Yushima, Bunkyo-ku, Tokyo, 113-8510, Japan.

Acknowledgements:
We thank T. Shimada, R. Mizuno, Reiko Hira for animal husbandry and genotyping, M. Kawabata, A. Rios, T. K. Fujita, Sakairi, S.L. Smith, J.N. Stirman, S. Aoki, A. Funamizu K. Ishizu, S. Tsutsumi, M. Morishima, T. Ishikawa, T. Yamazaki, H. Mori for technical advices and discussion. This work was supported by JP22wm0525007 (RH), JP19dm0207089 (YI) from AMED, JP22H02731 (RH), JP20K22678 (RH), JP21B304 (RH), JP21H05134 (RH), JP21H05135 (RH), JP16H06276 (YI), JP21H0524 2(YI), JP19H03342 (YI), JP23H02589 (YI), and JP20H05053 (YI) from MEXT/JSPS, JPMJCR1751 (YI) from JST, Nakatani Foundation (RH), Shimadzu Foundation (RH), Takeda Science Foundation (RH), Takeda Science Foundation (YI), The Precise Measurement Technology Promotion Foundation (RH), Tateishi Science and Technology Foundation (RH), and Research Foundation for OptoScience and Technology (RH).

Author contributions:
R.H. conceived the project. T.Y., H.S. M.T. conducted electrophysiological experiments. S.T. conducted anatomical experiments. R.H., T.Y., H.S. M.T. analyzed electrophysiological data. H.Y., J.I., R.H. performed spiking neuron network simulations. R.H. built and analyzed the reservoir model. T.Y., R.H. built the scanning optogenetics system. Y.I. supervised the project. R.H. wrote the paper with the comments of all authors.

Abstract

The cerebral cortex, cerebellum, and basal ganglia play a central role in flexible learning in mammals. However, how these three structures work together is not fully understood. Recently, it has been suggested that reinforcement learning may be implemented not only in the basal ganglia but also in the cerebellum, as the activity of cerebellar climbing fibers represents reward prediction error. If the same learning mechanism via reward prediction error occurs simultaneously in the basal ganglia and cerebellum, it remains unclear how these two regions co-function. Here, we recorded neuronal activity in the output of cerebellum and basal ganglia, the cerebellar nuclei and substantia nigra pars reticulata, respectively, from ChR2 transgenic rats with high-density Neuropixels probes while optogenetically stimulating the cerebral cortex point-by-point. The temporal response patterns could be categorized into two classes in both cerebellar nuclei and substantia nigra pars reticulata. Among them, the fast excitatory response of the cerebellar nuclei due to the input of mossy fibers and the inhibitory response of the substantia nigra pars reticulata via the direct pathway were synchronized. This coincidence, reproduced in a spiking network simulation based on connectome data, was expected to synchronously activate the cerebral cortex via the thalamus. To further investigate the significance of this synchronous positive feedback, we constructed a reservoir model that mimics the time course of the activity dynamics of cerebral cortex and temporal responses of cerebellar nuclei and substantia nigra pars reticulata. Plasticity of both parallel fiber inputs to Purkinje cell and corticostriatal synapses onto the striatal neurons of the direct pathway was essential for successful learning of a reinforcement learning task. Notably, learning was inhibited when the timing of the cerebellar or basal ganglia output was delayed from the real data by 10 ms; the larger this delay, the slower the learning rate. This necessary temporal precision was observed only when the cerebral cortex operated in the β-to-γ frequency range. These results indicate that coordinated output of the cerebellum and basal ganglia, with input from the cerebral cortex in a narrow frequency band, facilitates brain-wide synergistic reinforcement learning. Thus, our findings contribute to a holistic understanding of the interactions among the cerebellum, basal ganglia, and cerebral cortex.

Introduction

The brain is a complex system composed of many unique information-processing regions that operate in a coordinated manner to produce flexible and sophisticated behavior (Doya 2000, Shadmehr and Krakauer 2008, Penhune and Steele 2012, Caligiore, Pezzulo et al. 2017, Lake, Ullman et al. 2017, Caligiore, Arbib et al. 2019). To understand the mechanism of cooperative information processing, it is necessary to elucidate how the multiple interregional loop circuits work together. The cerebral cortex outputs to numerous subcortical structures, including the cerebellum and basal ganglia. These regions differ in many evolutionary and functional aspects but are similar in the fact that they send signals back to the cerebral cortex via the thalamus (Allen and Tsukahara 1974, Schell and Strick 1984, Alexander and Crutcher 1990, Kebschull, Richman et al. 2020, Grillner 2021). These multi-synaptic pathways, each with its own specific microcircuits and integration strategies, substantially affect ongoing activity of the cerebral cortex and entire brain.

Cerebellar nuclei (CN) are the output nuclei of the cerebellum and have direct thalamic projections, receiving inhibitory inputs from Purkinje cells (PCs), which are activated by excitatory granule cells that receive excitatory mossy fiber (MF) inputs. MFs are activated directly from the cerebral cortex, and consequently many neurons in CN receive inhibitory inputs from the cerebral cortex. MFs also directly excite CN neurons (Shinoda, Sugiuchi et al. 1992, Sugihara, Wu et al. 1996). Thus, CN receive multi-phase excitatory and inhibitory input from the cerebral cortex. The substantia nigra pars reticulata (SNr), an output nucleus of basal ganglia, is composed of inhibitory neurons projecting to the thalamus. In the SNr, a triphasic response to cerebral cortex stimulation in the order of excitation, inhibition, and excitation has been characterized in detail (Nambu, Tokuno et al. 2000, Chiken, Shashidharan et al. 2008). To understand how these responses with excitatory and inhibitory dynamics are reintegrated in the thalamus and cerebral cortex, the relationships between multiple cerebral cortex areas and the subdivisions within cerebellum and basal ganglia should be systematically examined under identical conditions.

Coordination of cerebro-cerebellar loop plays an important role in cognitive and motor tasks (Proville, Spolidoro et al. 2014, Gao, Davis et al. 2018, Chabrol, Blot et al. 2019, Wagner, Kim et al. 2019, Zhu, Hasanbegović et al. 2023). Coordination of cerebro-basal ganglia thalamocortical loop is also critical in normal behavior and in pathological conditions (Alexander, DeLong et al. 1986, Alexander and Crutcher 1990, Yasoshima, Kai et al. 2005, Stein and Bar-Gad 2013, Wang, Yin et al. 2021, Yoshizawa, Miyamura et al. 2023). Classically, the basal ganglia and cerebellum were thought to be responsible for reinforcement and supervised learning, respectively (Doya 1999). However, the cerebellum has recently been shown to be also capable of reinforcement learning, as complex spikes in PCs are associated with reward prediction errors (Thoma, Bellebaum et al. 2008, Heffley and Hull 2019, Yamazaki and Lennon 2019, Sendhilnathan, Semework et al. 2020, Kostadinov and Häusser 2022, Hoang, Tsutsumi et al. 2023). Thus, plastic changes in parallel fiber input in PCs due to climbing fibers input and plastic changes in corticostriatal pathways due to dopamine release could both lead to reinforcement learning. As circuit changes generated by different mechanisms facilitate learning, they must be consistently reintegrated in the cerebral cortex via the thalamus for decision making and motor output.

The cerebellum and basal ganglia each exhibit unique oscillatory activities (Courtemanche, Robinson et al. 2013, Halje, Brys et al. 2019). For example, cerebellar oscillations in the β band range (15–30 Hz) is crucial for regulating action timing in human (Spencer and Ivry 2021). γ oscillations (30–80 Hz) can be also generated by cerebellar cortical circuitry (Middleton, Racca et al. 2008). β oscillation is simultaneously enhanced in cerebral cortex and basal ganglia when

determining motor output in rats (Leventhal, Gage et al. 2012). In motor cortex and basal ganglia, the β band oscillation is enhanced during reaching, grasping and other motor tasks (Khanna and Carmena 2015). The excessive β oscillation is observed in patients of Parkinson's disease (Morén, Igarashi et al. 2019, Gambosi, Sheiban et al. 2024). Thus, both the cerebellum and basal ganglia exhibit oscillations in the β-γ range, and their proper timing and amplitude are essential for behavioral coordination. The close frequency band activity of the cerebellum and basal ganglia may contribute to the coordinated information processing of the entire brain (Diedrichsen, Ivry et al. 2003, Petter, Lusk et al. 2016, Tanaka, Kameda et al. 2024).

In this study, we investigated the propagation of neural activity patterns of the cerebellum and basal ganglia in response to cerebral cortex photoactivation using high-throughput optogenetic stimulation (Hira, Honkura et al. 2009, Hira, Ohkubo et al. 2013, Hira, Terada et al. 2015) and neuronal activity recordings with the high-density Neuropixels probes (Jun, Steinmetz et al. 2017). Although the temporal response patterns differed, CN excitatory signals and SNr disinhibitory signals were synchronously elevated. We modeled these circuits with a spiking neuronal network based on connectome data and a reservoir-based reinforcement learning model and analyzed these synergistic features. The results indicate that the synergy can facilitate brain-wide consistent reinforcement learning.

Results

A high-throughput optogenetic system

Transcranial optogenetic stimulation of cerebral cortex and neuronal recordings in CN and SNr

To stimulate large cortical areas in a point-by-point manner and to make comparisons between stimulated areas, we used transgenic rats (Saiki, Sakai et al. 2018, Mitani, Kawabata et al. 2022) densely expressing ChR2 under the Thy1.2 promoter in all layers of the cerebral cortex under head-fixed conditions in the awake state. We previously reported a method enabling photostimulation of ChR2-expressing neurons in mice with retained skulls (TOS, transcranial optogenetic stimulation) (Hira, Honkura et al. 2009, Hira, Ohkubo et al. 2013, Hira, Ohkubo et al. 2013, Hira, Terada et al. 2015). For optical stimulation of the rat cerebral cortex, the area that can be stimulated must be expanded. Therefore, we simulated the optical pathway and constructed a system with a photostimulation area of 10 mm × 10 mm based on the simulation results (**Fig. 1a–e**). We confirmed that photostimulation with our new system was possible in the transgenic rats by maintaining the transparency of a thinned skull in one hemisphere of the dorsal cerebral cortex (**Fig. 1f–j**). To determine the resolution of photostimulation, we stimulated neurons in the cerebral cortex with a 445 nm laser and recorded the surrounding spiking activity. A fast response of < 1 ms latency was observed in neurons < 0.5 mm from the center of optical stimulation (**Fig. 1k**), indicating that direct photostimulation occurred within 0.5 mm from the center of photostimulation.

We divided a 10 mm × 10 mm area including a thinned-skull portion into 32 × 32 points and illuminated each point with a focused blue laser for 5 ms (**Fig. 1f**). We recorded CN and SNr neural activity using Neuropixels probes (Jun, Steinmetz et al. 2017). In total, 544 and 282 neurons were isolated in CN (9 rats, 23 sessions) and SNr (8 rats, 19 sessions), respectively. We examined the exact recording location of each channel with histological data and local field potential (LFP) correlation structures. We identified the location of all recorded neurons at the level of subdivision of each region or layer (interposed or lateral nuclei for CN, molecular layer, granule cell layer, PC layer, white matter for neurons in the cerebellar cortex, medial (< 2mm from midline) or lateral (≥2 mm from midline) portion for SNr,).

Responses of a representative neuron recorded at lateral CN are shown in **Fig. 1l,m**. We displayed the average firing rate between 0–50 ms from the stimulus at each point on a color scale (hereafter referred to as the response map, **Fig. 1l**). The response map indicated that the neuron received the input from the primary sensory cortex (S1), primary motor cortex (M1), and secondary motor cortex (M2). We called the stimulation points that significantly affected the firing rates of recorded neurons the "receptive field" of the neuron. A raster plot and peri-stimulus time histogram (PSTH) for the receptive field are shown in **Fig. 1m**. We performed this analysis on all neurons and identified responsive neurons that had receptive fields.

Two types of response classes in CN neurons

To identify CN neurons, DiI fluorescence dye was applied to the Neuropixels probes, and the probe trajectories were identified histologically (**Fig. 2a**). We used 384 electrodes every 20 mm to skip one recording site, so that the recordings were linear over 7.5 mm. LFP correlation analysis revealed multiple clusters, which corresponded well with the histological layer structure and nuclear boundaries. In particular, we found the bird sign of the LFP (***** in **Fig. 2a**) enabling us to separate CN from their surroundings (see Methods). This corresponds to the fact that CN are located in white matter and are highly correlated with signals from white matter.

We identified two representative CN response classes. A typical class 1 response was a strong inhibitory response followed by an excitatory response (**Fig. 2b**), whereas a typical class 2 response was transient excitation (**Fig. 2c**). K-means clustering (K = 6) of z-scored temporal response patterns of all responsive CN captured these two clusters: clusters #1 and #2 for class 1, and clusters #3 and #4 for class 2 (**Fig. 2d**). In clusters #1 and #2 (class 1), the onset and peak latency of inhibitory responses were 13.1 ± 0.6 ms and 41.2 ± 3.3 ms, respectively, and the onset and peak latency of excitatory responses were 58.9 ± 3.2 ms and 94.6 ± 2.9 ms, respectively. Neurons with class 1 response accounted for 56.7% (72/127) of all neurons. In clusters #3 and #4 (class 2), the onset and peak latency of excitatory responses were 14.0 ± 0.7 ms and 23.9 ± 0.4 ms, respectively. The excitatory peak of class 2 responses was significantly faster than that of class 1 inhibitory responses ($p = 2.9 \times 10^{-12}$, Wilcoxon's rank-sum test). Neuron with class 2 response accounted for 30.7% (39/127) of all neurons. Thus, neurons with class 1 and class 2 responses cover the majority (87.4%, 111/127) of CN responsive neurons. Neuron with class 1 response had a higher spontaneous firing rate than the neuron with of class 2 response (37.9 ± 2.0 Hz vs. 27.6 ± 4.0 Hz, p = 0.0053, Wilcoxon's rank-sum test), suggesting that neurons with class 1 and 2 responses have distinct biophysical properties.

It is unclear whether neurons with class 1 and class 2 responses are two completely different groups of neurons or whether a single neuron has both properties. Notably, some neurons exhibited mixed responses of class 1 and class 2. A neuron that was classified as class 1 had a transient fast excitatory response resembling class 2 only when S1 was stimulated (**Fig. 2e–g**). In other words, the class 2 response pattern was added only in S1, on top of the inhibitory to excitatory response pattern typically observed in class 1. Another neuron that was classified as class 1 had a class 2-like fast transient excitatory response when M2 or S1 was stimulated (**Extended Data Fig. 1a–c**). Thus, class 1 and 2 responses can merge within a single neuron. Distinct response patterns depending on the stimulation areas indicate that CN can integrate the activity of multiple cortical areas in a manner that reflects area-specific time series information.

Furthermore, it is unclear whether the different response patterns of class 1 and class 2 depended on the location of stimulation or recording. The class 1 excitatory and inhibitory responses and the class 2 excitatory responses were evoked by a wide area of M2, M1, and S1, with no clear differences (**Fig. 2h**). The receptive fields of class 1 inhibitory and class 2 excitatory responses had receptive fields of up to 4–5 mm^2, with no clear differences (**Fig. 2i**). By contrast, more class 1 responses were observed in the lateral nucleus than in the interposed nucleus ($p = 3.8 \times 10^{-3}$, χ^2-test), whereas more class 2 responses were observed in the interposed nucleus than in the lateral nucleus (p = 0.040, χ^2-test; **Fig. 2k**). Thus, CN response patterns depend more on the location of the recording than that of the stimulus.

Recordings of PCs and MFs explain responses of CN neurons

There are multiple possible pathways from the cerebral cortex to the CN, and the pathways through which neurons with class 1 and 2 responses are generated remain unclear. We measured the activity of two structures that enter CN: MFs and PCs. MFs exhibit characteristic short waveforms of axonal activity and negative after waves (NAW) (Van Kan, Gibson et al. 1993, Prsa, Dash et al. 2009, Van Dijck, Van Hulle et al. 2013, Muzzu, Mitolo et al. 2018, Beau, Herzfeld et al. 2024). We determined MFs by waveform features and the observed layer. Most MFs showed very fast transient excitatory responses to cortical stimulation (**Fig. 3a,b**). Inhibitory responses were observed in five MFs, whereas 87 MF excitatory responses had an onset and peak latency of 11.0 ± 0.5 ms and 21.4 ± 0.9 ms, respectively, which were significantly faster (by 3 ms and 2.5 ms) than those of class 2 CN (onset: $p = 7.0 \times 10^{-6}$; peak: $p = 3.0 \times 10^{-5}$, Wilcoxon's rank-sum test; **Fig. 3g**). These results are consistent with

the idea that fast excitatory responses of class 2 CN were via MF input, which is also anatomically plausible.

PCs are characterized by simple spike (SS) and complex spike (CS). We analyzed these two types of spiking activity separately. All complex spikes showed transient activity with jitter in a very narrow range (**Fig. 3c,d**; onset latency, 15.0 ± 0.6 ms, range, 12–19 ms; peak latency, 23.4 ± 0.7 ms, range, 20–28 ms). Notably, the cortical areas that elicited complex activity were confined to a portion of frontal cortex (**Fig. 3d**, left), and S1 rarely evoked complex spikes. SSs showed broad responses compared with complex spikes (**Fig. 3e,f**). The onset and peak latency were 15.4 ± 1.7 ms and 35.3 ± 3.1 ms, respectively. These values are comparable to those of class 1 inhibitory responses of CN. Additionally, the duration of the excitatory responses was roughly similar to that of CN class 1 inhibitory responses. Interestingly, the mean SS response had a transient decrease of firing activity 20–46 ms after photostimulation. This is compatible if the CS, which has a peak latency of 23.4 ms, pauses the SS for approximately 20 ms. We also examined the cross-correlograms of three putative SSs and three CN neurons in simultaneous recordings and found monosynaptic inhibition from SSs of PCs to CN neurons with class 1 response (**Fig. 3h,i**). Furthermore, the maps of inhibitory responses of CN and the maps of SS excitation overlapped (**Fig. 3j**). Similar result was observed in the other rat (**Extended Data Fig. 1d-f**). Thus, monosynaptic inhibition from SS to CN neuron with class 1 response may directly contribute to the strong suppression of CN neurons with class 1 response after photostimulation.

As the broad excitation after inhibition in class 1 response was not caused by MFs or PCs, it was most likely due to rebound excitation (Aizenman and Linden 1999, Hoebeek, Witter et al. 2010). By contrast, we found a CN neuron whose excitation after inhibitory activity differed across cortical areas (**Fig. 3k–m**). This neuron exhibited an increased excitatory response after photostimulation of M1 (blue, purple) but not M2 (red) or S1 (orange). Thus, the responses can switch in a region-specific manner. In summary, class 1 excitatory responses appear to be a rebound; however, the underlying process is complex, and the cerebral cortex may use this excitation to transmit region-specific information. Taken together, we illustrated the circuitry for phase 1 (excitation of class 2 responses), phase 2 (inhibition of class 1 responses), and phase 3 (excitation of class 1 responses) (**Fig. 3n**).

Two types of response classes in SNr neurons

Next, we examined the pattern of transmission from the cerebral cortex to the SNr, an output nucleus of the basal ganglia. We histologically confirmed the recording location (**Fig. 4a**). We identified two types of response classes in SNr neurons. Typical neurons with class 1 responses showed a clear triphasic pattern similar to that of previous studies (**Fig. 4b**) (Fujimoto and Kita 1992, Kitano, Tanibuchi et al. 1998, Nambu, Tokuno et al. 2000, Nambu, Tokuno et al. 2002, Sano, Chiken et al. 2013). The triphasic response consisted of an excitatory-inhibitory-excitatory activity sequence in which the third excitatory response was always larger than the first one, and the firing activity was often completely suppressed during the second inhibitory phase. We also found a monophasic excitatory response (class 2) (**Fig. 4c**). K-means clustering (K = 6) of z-scored temporal response patterns of all responsive SNr neurons roughly captured these two classes: clusters #1 and #2 for class 1, and clusters #3 and #4 for class 2 (**Fig. 4d**). Neurons with class 1 (24/56) and class 2 (25/56) responses cover the majority (87.5%, 49/56) of SNr neurons.

We further investigated whether neurons with class 1 and class 2 responses are two completely different groups of neurons or whether a single neuron has both properties. One neuron with a class 1 response showed the triphasic response only when the frontal area was stimulated but showed a monophasic excitatory response when more posterior cortical areas were stimulated (**Fig. 4e**). Another

neuron also showed a mixed response; however, class 1 and 2 responses were induced by the posterior and anterior part of the receptive field, respectively (**Fig. 4f**). These data are consistent with the idea that SNr can integrate information from different cortical areas with distinct patterns of activity transmission.

Some neurons only showed a fast excitatory response that had similar time courses to the first excitatory response of the class 1 triphasic response (**Fig. 4g**), an inhibitory response similar to the second inhibitory phase of the triphasic response (**Fig. 4h**), and an inhibitory-excitatory response pattern similar to the second and third phases of the triphasic response (**Fig. 4i**). Thus, the activities of neurons in SNr were characterized as based on the triphasic response, of which parts were missing (Nambu, Chiken et al. 2023).

We further examined the dependencies of the response patterns on the locations of stimulation and recording. The excitatory source areas for neurons with class 1 and 2 responses distributed over a wide area of M2, M1, and S1 (**Fig. 4j**). Cluster #1 neurons in SNr also received inhibitory input from wide cortical areas including M2, M1, and S1 (**Fig. 4k**). In clusters #1, #2, and #3, the sizes of the excitatory and inhibitory receptive fields were 3–4 mm^2 and 1–2 mm^2, respectively (**Fig. 4l**), supporting the center-surround model (Nambu, Tokuno et al. 2000). By contrast, more triphasic or inhibition-excitation responses were observed in the lateral SNr (>2 mm lateral from bregma) than in the medial SNr ($p = 0.014$, χ^2-test; **Fig. 4m**). Thus, response patterns in SNr depend more on the location of the recording than the stimulus. Of note, the medial SNr may also receive more triphasic input from higher-order regions, such as the prefrontal cortex and orbitofrontal cortex (Maurice, Deniau et al. 1999), which were not stimulated in our experiment.

We investigated what anatomical pathways each pathway is composed of. Cross-correlograms of SNr neurons showed rare inhibitory interactions (**Extended Data Fig. 2a**). However, this inhibition does not explain the pattern of cortical responses to stimuli. The lateral inhibition inside the SNr does not seem to be large enough to shape the response patterns to cortical input. Based on previous studies (Fujimoto and Kita 1992, Nambu, Tokuno et al. 2000, Nambu, Tokuno et al. 2002, Sano, Chiken et al. 2013), our data is consistent with the following circuit. The hyperdirect pathway runs from the cerebral cortex to the subthalamic nucleus to the SNr and is composed of fast transient excitation. The direct pathway inhibits SNr via the striatum. The indirect pathway activates the SNr after the hyperdirect and direct pathway inputs. The direct pathway can disinhibit the thalamus and cortex and makes a positive feedback loop between the cerebral cortex and basal ganglia. The hyperdirect pathway and indirect pathway localize the direct pathway spatiotemporally, resulting in a feedback circuit in which the cerebral cortex is continuously gated by the SNr (**Extended Data Fig. 2b**).

Retrograde tracing experiment

To determine which thalamic nucleus the SNr or CN neurons at the location we recorded project to, we injected AAV-based retrograde tracer (Tervo, Hwang et al. 2016) (AAVretro-CAG-tdTomato) into the thalamus of Thy-1 ChR2 transgenic rats (**Fig. 5a**). Injections into the VL resulted in many tdTomato-labeled neurons in the bilateral CN but only a few in SNr (**Fig. 5c–f**). Within CN, labeled neurons were observed in the medial, interposed, and lateral CN bilaterally, but was brighter in the contralateral than the ipsilateral CN. In the contralateral cerebellum, axons collateral of CN neurons in the white matter and granule cell layer were also clearly labeled (**Fig. 5g,h**). We also confirmed tdTomato-positive neurons in layers 5 and 6 of the motor cortex (**Fig. 5i,j**). After injection of VM, tdTomato-labeled neurons were observed in the ipsilateral SNr at 2.1–2.6 mm lateral to the bregma (but not in the medial SNr) and in medial, interposed, and lateral CN bilaterally (**Fig. 5k–o**). After injection of VA, tdTomato-labeled neurons were observed in the ipsilateral SNr at 1.4–2.6 mm lateral

to the bregma and in medial, interposed, and lateral CN bilaterally (**Fig. 5p–t**). In all cases, contralateral CN were more densely labeled than ipsilateral CN, whereas contralateral SNr was not labeled. These results indicate that the neural activity of the CN propagates to the VL, VA, and VM, and that the activity of the lateral SNr propagates to the VM and VA, which is largely consistent with previous studies (Kuramoto, Furuta et al. 2009, Kaneko 2013, Kuramoto, Ohno et al. 2015, Gornati, Schäfer et al. 2018).

Cerebellar output to the thalamus, motor cortex, and striatum

The cerebellum and basal ganglia have direct connections that do not involve the cortex via thalamus (Ichinohe, Mori et al. 2000, Bostan and Strick 2018, Yoshida, Oñate et al. 2022). The excitatory response of the CN when stimulated by the cerebral cortex might be transmitted to the striatum via the thalamus with a short latency (Chen, Fremont et al. 2014). To investigate the fast propagation of activity from the cerebellum to the basal ganglia, we conducted electrophysiological recordings of the CN, motor cortex, dorsolateral striatum (DLS), and dorsomedial striatum (DMS) during cerebellar stimulation (**Fig. 6**). We analyzed the neurons significantly increased the firing rate within 10 ms after photostimulation. Oblique laser incidence from behind the cerebellum through the transparent skull produced a very fast latency response (< 10 ms) in response to photostimulation (3.3 ± 0.40 ms, 8/37 neurons) (**Fig. 6g-i**). We confirmed that the CN neurons of the same transgenic rats express ChR2. The area where this response was detected covered the size of the CN (**Fig. 6g**), indicating direct stimulation of ChR2 on the soma or axons extending into the cerebellar cortex (**Fig. 5e**). We found evoked activity with a latency of < 10 ms in the VL (**Fig. 6j-l**; 5.0 ± 0.11 ms), CL (**Fig. 6m-o**; 5.4 ± 0.27 ms), motor cortex (**Fig. 6p-r**; 5.6 ± 0.27 ms) and striatum (**Fig. 6s-u**; 5.1 ± 0.40 ms; DLS or DMS). This indicates that the fast latency activity in DLS and DMS could be caused through the CN-thalamus-striatum pathway without going through the motor cortex. However, only 4.8% (6/126) of DLS and 4.1% (7/172) of DMS neurons responded to CN stimulation with a latency of < 10 ms, indicating that this CN-to-striatum activity propagation occurred only in a limited number of neurons. In fact, > 100 ms long-lasting activity was not often observed in SNr but in CN upon cerebral cortex stimulation. Thus, although this pathway has important functions in many aspects (Alexander, DeLong et al. 1986, Ichinohe, Mori et al. 2000, Yoshida, Oñate et al. 2022), we will not consider it in the present study.

Hypothesis on brain-wide temporal integration

As CN→thalamus is excitatory and SNr→thalamus is inhibitory, increases in CN activity and decreases in SNr activity positively affect the thalamus. Notably, the excitation of class 2 response and the transient inhibition of the second phase of class 1 SNr response should coincidently activate the thalamus, as both of them two occur 20–30 ms after cortical stimulation (CN, **Fig 2d;** SNr, **Fig 4d**). Moreover, these two receptive fields almost overlapped (**Fig. 2i; Fig. 4j**). Therefore, a few tens of ms after the activity of a particular cortical area, signals that have passed through the SNr and CN circuits feedback synchronously to the cerebral cortex via the thalamus. We hypothesized that this synchronous positive feedback is the key to understand the brain-wide dynamics and learning. How the influence returns to the thalamus and cortex via the cerebellum and basal ganglia cannot be clarified experimentally because it is expected to be obscured by the mixture of various signals in the thalamus. Accordingly, in the next section, we performed computer simulations to investigate how this brain-wide synchronous circuit works in a coordinated manner.

Spiking neural network reproducing representative activity of CN and SNr

Next, to investigate whether the activity propagation through these six pathways aligns with connectome data, we constructed spiking networks for the basal ganglia and cerebellum (**Fig. 7a,b; Extended Data Fig. 3a; Extended Data Table 2**). For the basal ganglia, we built a spiking neural network based on the connectome data using the Izhikevich model (Izhikevich 2003) (**Extended Data Fig. 3b;** see **Methods**). This network contained the striatum, subthalamic nucleus, external globus pallidus, SNr, and thalamus (VL, VM, and parafascicular nucleus (PF)). The model reproduced a triphasic response to cerebral cortical stimulation in SNr neurons. To estimate which pathways from the cerebral cortex to SNr contribute to each phase of the triphasic response, we conducted virtual blocking experiments of synaptic connections (**Fig. 7c**). Blocking the hyperdirect pathway (i.e., monosynaptic input to the subthalamic nucleus from the cerebral cortex) eliminated the initial short excitatory response. Blocking the direct pathway abolished the second phase and weakened the third phase. Blocking the indirect pathway weakened the third phase.

Regarding the relationship between the cerebral cortex and cerebellum, it has been reported that the topography of the cortex is maintained particularly in the outputs from the pontine nuclei (Wu, Sarpong et al. 2023). However, this topography may be largely disrupted from granule cells to PCs (Pisano, Dhanerawala et al. 2021). Therefore, instead of creating a network model at a submodule level equivalent to that of the basal ganglia, we created a single module model for the cerebellum. We constructed a simulation consisting of MFs, granule cells, molecular layer interneurons, Golgi cells, PCs, and CN (**Fig. 7a,b; Extended Data Table 2**). This model replicated the activity of class 1 and class 2 responses in CN (**Fig. 7d**). We conducted virtual blocking experiments as well. By blocking the projections from pontine nuclei to CN, only class 2 transient excitatory responses were eliminated. Blocking the synaptic functions from PCs to CN abolished class 1 responses. Therefore, CN neurons with class 1 inhibitory responses were inhibited by the PCs and then rebounded after inhibition in this model. Overall, our simulation replicated our electrophysiological results based on our current understanding of rodent brain circuits.

Integration of two loop circuits during ongoing activity

To examine how the CN and SNr responses merged, we added projections from CN and SNr to the thalamus. Based on the results of tracer experiments, we assumed that VM receives both inputs from SNr and CN, while VL only received input from CN. We also assumed here that these thalamic neurons do not receive direct input from cerebral cortex. Approximately 30 ms after photostimulation, both thalamic activities were elevated (**Fig. 7e**). VL showed second peak of activity. To investigate how these thalamic activities can merge in the cerebral cortex, we simulated layer 5 pyramidal neuron (L5PN) receiving both inputs (Hooks, Mao et al. 2013, Kaneko 2013). Again, we assumed that this neuron does not receive input from surrounding cortical neurons. The L5PN showed triphasic responses, where the first excitatory signal was the summation of the direct pathway and CN phase 1 activities, the second inhibitory signal was the summation of the indirect pathway and CN phase 2 activities, and the third excitatory signal was CN phase 3. To investigate whether the synchronization of direct pathway and MF-CN pathway plays a role in information integration, we changed the axon conduction time of either corticostriatal and cortico-subthalamic projections or corticopontine and cortico-olivary projections (**Fig. 7f,g**). The exact synchronization at the timescale of 10 ms enhanced the summation of the CN and SNr outputs approximately 40 ms after the stimulation of cerebral cortex at the L5PN. Thus, our simulation reveals the importance of the temporal dynamics of outputs from the cerebellum and basal ganglia for information transmission back to the cerebral cortex via the thalamus. In the real brain, the interactions between thalamus and cortex that we have neglected would be complex. Synchronization of signals through the cerebellum and basal ganglia would be additive

on top of such activity, thus controlling neurons in the cortex.

Reservoir-based reinforcement learning model

Finally, we examined how the interaction of cortico-cerebellar and cortico-basal ganglia circuits contributes to learning. Recent studies have shown that in addition to dopamine neurons in the basal ganglia, complex spikes in cerebellar PCs reflect reward prediction error (Thoma, Bellebaum et al. 2008, Heffley and Hull 2019, Sendhilnathan, Semework et al. 2020, Kostadinov and Häusser 2022, Hoang, Tsutsumi et al. 2023). This indicates that reinforcement learning should progress in both the basal ganglia and cerebellum. Thus, we investigated how reinforcement learning, which progresses in these different systems, merges coherently.

We built a model in which the activity of the cerebral cortex was represented by a reservoir of 800 units with a time constant of 20 ms and that produced complex dynamics in response to an auditory cue and reward inputs (**Fig. 8a**). For the basal ganglia, we assumed that the output is the result of convolving cerebral cortex activity with pathway-specific filters in the hyperdirect, direct, and indirect pathways (**Fig. 8b**, left). Similarly, for the cerebellum, the output was assumed to be the result of convolving the reservoir output with filters corresponding to CN phases 1, 2, and 3 (**Fig. 8b**, right). These six filters were made to tightly reproduce the experimental data.

Using this circuit, we trained a simple reinforcement learning task (**Fig. 8c**). The agent had to pull or hold a lever to get a reward. When it held the lever for 1 s, the tone cue was presented. The agent had to pull the lever within 0.3 s after the tone cue to get a reward. The decision to pull or hold the lever was made by comparing the pull value and hold value. The pull value was defined as the sum of the output results from the direct pathway, phase 1, and phase 3, since the activity of these pathways would enhance thalamic and cortical circuits leading to the pull behavior. The hold value was defined as the sum of the output results from the hyperdirect pathway, indirect pathway, and phase 2. These values were converted to lever pull probability using a sigmoid function, and based on this, the decision to pull or hold was made every 0.1 s. As pulling the lever requires force, a bias term was added to the sigmoid function to make pulling less likely. The final behavioral output, determined by integrating the outputs of the basal ganglia and cerebellum, was assumed to occur in the M1 via the thalamus. Synaptic plasticity occurred based on reward prediction error on corticostriatal synapses of the direct pathway and PF-PC synapses. Positive and negative reward prediction error (RPE) induced LTP and LTD in corticostriatal synapses, respectively, and LTD and LTP in PF-PC synapses, respectively (see **Methods**).

The simulation results show that the agent increased the reward acquisition rate during a 20 min training period (**Fig. 8d**). During this time, the pull value increased and hold value decreased immediately after the sound, whereas the pull value decreased and hold value increased during the holding period. In accordance with this, 200 ms after the tone presentation, the activities of the striatal direct pathway and cerebellar phase 2 pathway increased and decreased, respectively (**Fig. 8e**), whereas 600 ms after the tone presentation, these changes were milder (**Fig. 8f**). Thus, synaptic plasticity of both pathways occurred in a coherent manner to induce efficient behavior. Note that this model predicts that the triphasic activity patterns in response to cerebral cortex activity change from early to late learning stages (**Fig. 8e,f**, right).

Next, we blocked the plasticity of either the basal ganglia or cerebellum. As a result, the reward acquisition rate significantly decreased in both cases, indicating that the plasticity of both structures is important for learning in this model (**Fig. 8g**).

Furthermore, to investigate whether the precise timing of the outputs from the basal ganglia and cerebellum contributes to learning, we delayed the output timing of the basal ganglia or cerebellum

(**Fig. 8h**). Notably, delaying the output of the basal ganglia or cerebellum by only 10 ms reduced the reward acquisition rate. The greater the delay (up to 70 ms), the lower the reward acquisition rate. Thus, we investigated how this time-delay effect relates to the frequency of cerebral cortex activity. We varied the time constants of neurons in 10 ms steps (from 10 ms to 50 ms) and found that the frequency band changed (**Fig. 8i**). When the time constant of a neuron was 10 ms, 20 ms, or 30 ms, delay-dependency was observed (**Fig. 8j**). These results suggest that delay-dependency requires a β- or γ-range timescale of cerebral cortex activity. These findings suggest that the mutual timing of responses from the basal ganglia and cerebellum, as observed in experimental data, is optimized for cooperative reinforcement learning between the two structures. This optimization has a greater impact when the timescale of cerebral cortex activity ranges from β to γ, which has been examined in detail in the motor cortex (Igarashi, Isomura et al. 2013, Popa, Spolidoro et al. 2013, Stein and Bar-Gad 2013).

Discussion

In this study, we used optogenetics and electrophysiological recordings, which revealed that the response patterns of most single neurons in CN and SNr to cortical stimulation can be categorized into two classes. In CN, we observed inhibition followed by excitation (CN class 1) and transient excitation (CN class 2). In SNr, we observed a triphasic response (SNr class 1) and monophasic excitation (SNr class 2). The timescale of CN responses was slower than that of SNr responses. The effects on the thalamus in total were expected in the order of inhibition-excitation-inhibition in SNr and excitation-inhibition-excitation in CN. Notably, the MF-CN pathway of the cerebellum and the direct pathway of basal ganglia were synchronized. The response patterns could be reproduced by a spiking neural network model of basal ganglia and cerebellum based on currently available connectome data. We developed a model in which the cerebral cortex is the reservoir, and reward prediction error signal prompts LTP of striatal direct pathway neurons and LTD of parallel fiber synapses onto PCs. We found that cerebellar and basal ganglia dynamics aligned with experimental data with an accuracy of 10 ms facilitated cooperative reinforcement learning. Moreover, the impact of temporal precision depended on the timescale of cerebral cortex activity. Overall, these data demonstrate a mechanism for the brain-wide synergy underlying consistent reinforcement learning in basal ganglia and cerebellum.

Previous computational studies have investigated the relationships among cerebral cortex, basal ganglia, and cerebellum (Houk and Wise 1995, Houk, Bastianen et al. 2007, Caligiore, Arbib et al. 2019). However, our model with reinforcement learning is the first model based on realistic temporal response patterns of the cerebellum and basal ganglia in response to cerebral cortex activation. Our detailed analysis of temporal activity patterns revealed that β- to γ-range activity of the cerebral cortex requires synergistic effects. These ranges in sensorimotor cortex have been observed during preparation and execution of voluntary movement (Igarashi, Isomura et al. 2013, Popa, Spolidoro et al. 2013, Stein and Bar-Gad 2013). Our model is also the first to assume that both the cerebellum and basal ganglia are engaged in reinforcement learning. Previously, it was assumed that the basal ganglia were responsible for reinforcement learning and the cerebellum for supervised learning, supposing a clear division of labor (Doya 1999, Doya 2000). Our model proposes a novel mechanism of linking multiple plasticity events across distinct brain regions. That is, the synapses that are thought to most often undergo plastic changes in the basal ganglia and cerebellum are pathways that synchronously send back signals from the cerebral cortex. This parallel circuit can coincide by inducing plasticity on the direct pathway and PF-PC synapses, allowing reinforcement learning to proceed consistently.

It is known that axons from VL and VM are distributed across the different layers of the cerebral cortex (Kaneko 2013). VM especially projects to apical dendrites in layer 1, whereas VL projects to the basal dendrites of L5 pyramidal neurons (Kuramoto, Ohno et al. 2015). Synchronous inputs to tuft and proximal dendrites within 20 ms enhance nonlinear integration, leading to dendritic spikes and bursting (Ledergerber and Larkum 2012, Poirazi and Papoutsi 2020). In the motor cortex, cortico-spinal neurons may detect this coincidence and directly convert it into motor output. Thus, if cerebellar and basal ganglia outputs are synchronized with a precision of 20 ms, activity of VL and VM could facilitate strong motor output via dendritic spikes in the motor cortex. This necessary timescale is consistent with the timescale that we have identified to promote thalamic activity in simulation and coordinated reinforcement learning in our model (i.e. β–γ range). Dendritic spiking may also induce synaptic plasticity, and simultaneous active input from the cerebellum (Popa, Velayudhan et al. 2013) and basal ganglia (Ueki, Mima et al. 2006) may facilitate circuit formation in the cerebral cortex. β–γ band oscillations are found in the motor cortex, basal ganglia, and cerebellum (Middleton, Racca et al. 2008, Leventhal, Gage et al. 2012, Courtemanche, Robinson et al. 2013, Igarashi, Isomura et al. 2013,

Khanna and Carmena 2015, Halje, Brys et al. 2019, Morén, Igarashi et al. 2019, Spencer and Ivry 2021). Taken together, we propose that the cerebellum, basal ganglia, and cortex acquire plasticity in a coordinated manner through β–γ rhythms, resulting in consistent behavioral decisions and reinforcement learning throughout the brain.

Whether the mechanisms of consistent reinforcement learning that we modeled here explain the actual brain's learning principle remains to be tested. As shown in **Fig. 8f**, excitatory transmission from CN to the thalamus and inhibitory transmission from the SNr to the thalamus will be larger and smaller, respectively, upon execution of the reinforced behavior after learning. By contrast, these transmissions will be smaller and larger, respectively, if the behavior does not need to be executed (**Fig. 8g**). It should be noted that CN and SNr activity in response to non-specific activation of the cerebral cortex will not change during learning. It is necessary to artificially stimulate cortical neurons to induce or suppress the behavior to be reinforced to verify these predictions. Moreover, optogenetic inhibition of PCs (whose activity is suppressed during the stimulation of cortical neurons that are involved in reinforced behavior) and optogenetic activation of striatal neurons in the direct pathway (whose activity is increased during the stimulation of cortical neurons that are involved in reinforced behavior) would cause the execution of the reinforced behavior via the thalamus and cerebral cortex. These experiments could be possible by combining an activity-dependent genetic switch (Lee, Hyun et al. 2017, Wang, Wildes et al. 2017) with appropriate opsins.

We have found that CN responses are categorized into distinct class 1 and 2 activities. The excitatory inputs in class 2 were thought to be via MFs (Tsukahara, Korn et al. 1968, Hesslow, Svensson et al. 1999, Wu, Sugihara et al. 1999); however, involvement via CFs (Sugihara, Wu et al. 1996) or disinhibition of PCs cannot be ruled out. Although many class 1 neurons did not show fast excitation, they can change to class 2 because MF-CN synapse potentiation can be induced by pairing with post-inhibitory rebound of CN neurons (Pugh and Raman 2008). As the MF-CN pathway is disynaptic, and the MF-granule cell-PC-CN pathway contains four synapses, the MF-CN pathway is considered faster. However, as indicated in **Fig. 2f** (* in the right panel), inhibition may precede excitation. Thus, even with signals starting simultaneously from the cerebral cortex, PCs may be able to alter the impact of the MF on the CN. CN phase 3 could represent post-inhibitory rebound excitation (Aizenman and Linden 1999, Hoebeek, Witter et al. 2010), excitation by internal circuits in CN, and reverberation by circuits not recorded in this study. A marked difference in the proportions of class 1 and class 2 in interposed and lateral CN could be due to the relative differences in MF and PC input. However, this requires further investigations in future studies.

Finally, we list below the limitations of this study and future directions. Convolution of the impulse response assumes a linear model; however, the brain is clearly not linear, and nonlinearities must be considered in many cases. We assessed the cerebellum and basal ganglia; nevertheless, other areas, such as the superior colliculus and sensory cortex, are also involved in decision making. We also disregarded the corticothalamic projection, even though the mechanisms by which inputs from the cerebral cortex merge with those from SNr and CN in the thalamus are most likely important. It is possible that rebound excitation of CN class 1 contributes to working memory maintained by the cerebro-cerebellar loop (Gao, Davis et al. 2018), which should be examined in the future. The mechanism by which the RPE is shared between the basal ganglia and cerebellum should also be clarified. As cooperation between the basal ganglia and cerebellum is important for facilitating learning throughout the brain, dysfunctions in one area may affect both areas. For example, diseases related to the basal ganglia, such as Parkinson's disease, obsessive-compulsive disorder, and Tourette's syndrome, may also be associated with the cerebellum as previously discussed (Caligiore, Pezzulo et al. 2017, Bostan and Strick 2018, Li, Le et al. 2023). Thus, our findings may call for re-interpretation

of various brain pathologies.

Methods

Animal preparation

All experiments were approved by the Animal Research Ethics Committee of the Institutional Animal Care and Use Committee of Tokyo Medical and Dental University (A2019-274) and were carried out in accordance with the Fundamental Guidelines for Proper Conduct of Animal Experiment and Related Activities in Academic Research Institutions (Ministry of Education, Culture, Sports, Science and Technology of Japan). We used 17 adult male and female rats (Thy1.2-ChR2-Venus transgenic rats, Long–Evans strain (Tomita, Sugano et al. 2009, Saiki, Sakai et al. 2018) at the age of 10-29 weeks for cerebellar recording and 10-14 weeks for SNr recording. These rats were kept under an inverted light schedule (lights off at 12 AM; lights on at 12 PM) in their home cages to adapt to experimental surroundings.

Surgery

Primary surgery was performed to attach a custom-made head-plate (Figure 2c) to the skull of rats under anesthesia by isoflurane gas (4.0–4.5% for induction and 2.0–2.5% for maintenance, Pfizer Japan, Tokyo, Japan) using an inhalation anesthesia apparatus (Univentor 400 anesthesia unit, Univentor, Zejtun, Malta). The body temperature was maintained at 37.0°C using an animal warmer (BWT-100, Bio Research Center, Aichi, Japan). The head of rats was fixed on a stereotaxic frame (SR-10R-HT, Narishige) with ear bars, and applied with lidocaine (Xylocaine Jelly, Aspen Japan, Tokyo, Japan) for local skin anesthesia and povidone-iodine disinfectant solution (10%, Kaneichi, Osaka, Japan) for disinfection around surgical incisions. The head-plate was then glued to the skull with stainless steel screws and dental resin cement (Super-Bond C & B, Sun Medical, Shiga, Japan; Unifast II, GC Corp., Tokyo, Japan). Reference and ground electrodes (PFA-coated silver wires, A-M systems, WA; 125-mm diameter) were implemented under the bone on the cerebellum. When we recorded the neurons in cerebellum, the reference electrode was placed over the anterior-most part of the cerebellum to avoid interference. Analgesics and antibiotics (meloxicam, 1 mg/kg sc, Boehringer Ingelheim, Tokyo, Japan; gentamicin ointment, 0.1% us. ext., MSD, Tokyo, Japan) were finally applied to remove pain and prevent infection.

More than three days later, secondary surgery was performed under the isoflurane anesthesia. For insertion of recording electrodes, we made a cranial window onto the cerebral cortex of left or right hemisphere or onto the cerebellum of the right hemisphere. The bone and dura mater were opened and removed by a dental drill (Tas-35LX, Shofu, Kyoto, Japan) and a dura picker (DP-T560-80, Bio Research Center, Aichi, Japan). The cortical surfaces were washed with PBS containing antibiotic (0.2% amikacin sulfate, Sawai, Osaka, Japan). We thinned the skull over the dorsal cerebral cortex and applied silicone oil to keep transparency for optogenetic stimulation (**Fig. 1f**). Thinned-skull area covered M1, M2, S1, and PPC. Because barrel cortex was not always completely covered with the thinned-skull window, we excluded the barrel cortex from S1 for the analysis when comparing the responsiveness. Analgesics (meloxicam, 1 mg/kg sc, Boehringer Ingelheim, Tokyo, Japan) was applied to remove pain.

Histology

After all recording sessions, the rats were perfused transcardially with saline and subsequent 4% formaldehyde in 0.1 M phosphate buffer under deep anesthesia with urethane (3 g/kg, ip, Nacalai Tesque, Kyoto, Japan) The brains were removed and then post-fixed with the same fixative for at least 12 h at 4° Celsius. The brains were removed and post-fixed with the same fixative for >2 days. The

brains were then embedded in 2 % agar in PBS and cut into sagittal sections with a thickness of 50 μm using a microslicer (VT1000S, Leica, Wetzlar, Germany). The serial sections were cover-slipped with mounting medium (DAPI Fluoromount-G, Southern Biotech, AL, USA). DiI, Venus, and DAPI (or NeuroTrace 435/455) were visualized through a fluorescence microscope (IX83 inverted microscope, Olympus, Tokyo, Japan).

Tracer study

Adult Thy1.2-ChR2-Venus transgenic rats (n = 6, male: 2, female: 4, 180-400 g) were used in this experiment. The rats were anesthetized with 2.5% isoflurane and an air flow of 0.2 liter per minute. Injection of AAVretro-CAG-tdTomato (Tervo, Hwang et al. 2016) (addgene, Plasmid #59462-AAVrg, 2.4×10^{12} GC/ml, 0.2 μL, 0.02 μL/min or 0.5 μL, 0.05 μL/min, 10 min) were performed (Hamilton, 10 μL Microliter Syringe Model #801 RN) at the VL (n=3, 1.7 mm left lateral to midline, 2.3 mm posterior to bregma, and 5.8-6.1mm deep from the brain surface), VM (n=2, 1.4 mm left lateral to midline, 2.4 mm posterior to bregma, and 6.9 mm deep from brain surface), or VA complex (n=1, 1.6 mm left lateral to midline, 1.7 mm posterior to bregma, and 6.0 mm deep from the brain surface) of thalamus by pressure through a glass micro pipette. Two weeks after AAV injection, the rats were anesthetized with urethane, and then perfused intracardially with saline and fixative solution containing 4 % paraformaldehyde. The Brain was quickly removed and fixed in 4% paraformaldehyde for 2 days at 4 °C then placed in a 30% sucrose in PBS solution for several days until they sank to the bottom of their container. The brain was then immediately immersed in isopentane over dry ice then stored at −80 °C until sectioned. Sagittal sections (20 μm or 50 μm) were obtained in a cryostat (NX50, Epredia) at -20°C through the cerebellar nuclei, SNr and thalamus.

Optogenetics

We simulated and assembled a scanning optical system with galvanometer mirrors (6210H, Cambridge Technology, USA) to systematically and rapidly photostimulate many areas of the cerebral cortex (**Fig. 1a-e**). Simulation of optical pathway was made with OpticStudio (version16.5, Zemax, USA) to illuminate an area of 10 mm × 10 mm, more than 150 mm away from the objective lens. This allowed us to put the electrode at the space between objective lens and the brain. After validation in the simulation environment, we built up scanning light pathway with SM2-based cage system (Thorlabs, USA) and the multifunction I/O device, USB-6259 (National Instruments, USA). Scan lens (EFL = 39 mm, LSM03-VIS, Thorlabs) and tube lens (two achromatic doublets (f = 400 mm, ACT508-400-A, Thorlabs) placed in a Plössl design) made an infinity-corrected laser light beam into the pupil of objective lens. We put a plano-concave lens (f = – 150 mm, LC1611-A, Thorlabs) just above the camera lens (Nikon, f=105 mm) to extend the working distance. We kept the diameter of the laser at pupil small enough (<0.1 mm) for achieving a large PSF extension in the Z-axis at each stimulus point. This minimized the light density shift due to the curvature of the rat cerebrum and at the same time reduce the light spreading conically inside the brain, thus creating a columnar illumination. For functional mapping of cerebral cortex, we stimulated 32 × 32 grid (323 μm spacing, total 1,024 points) with 115 ms interval pseudo-randomly for 15 cycles (Hira, Honkura et al. 2009, Hira, Ohkubo et al. 2013, Hira, Ohkubo et al. 2013, Hira, Terada et al. 2015). The stimulation point after the thin-skull point was always at bone, so that the stimulation interval of cerebral cortex was more than 230 ms. The stimulation point after the thin-skull point was always at bone, so that the stimulation interval of cerebral cortex was more than 230 ms. For functional mapping of cerebellum, we stimulated 32 × 32 grid (129 μm spacing, total 1,024 points) with 230 ms interval pseudo-randomly for 15 cycles. Recording during the stimulation at the bone was monitored as an internal control to discriminate with

any unnecessary effects including the neuronal activity via retinal light responses. We confirmed that there was no contamination of visually evoked activity in the responsive neurons that we analyzed. Each stimulation was 5 ms duration with 445 nm TTL-controllable diode laser (JUNO, Kyocera SOC, Japan). Laser power was set in each experiment sufficiently small not to induce movement when primary motor cortex was stimulated (0.7 mW–3.9 mW for stimulation of cerebrum, 15–21 mW for stimulation of cerebellum, at the center of field-of-view). Even at the edge of the field of view (7.1 mm from the center), the laser power was >85.7% of the center. All system was controlled with custom-made software written with LabVIEW (National instruments, USA)..

Electrophysiology

Right before the recording, the Neuropixels probes (Jun, Steinmetz et al. 2017) (IMEC, Belgium) were manually coated with lipophilic dyes, DiI (DiIC18(3), PromoKine, Heidelberg, Germany). The probes were fixed to a holder and handled using a micromanipulator (SM-15M, Narishige, Japan). Reference and ground electrodes were soldered, and attached to a custom-made part with four independent silver wires located under the skull onto the cerebellum. The probe was lowered in the coronal plane at 5–10 degrees from vertical at a speed of 10 μm/s until 8 mm below pia for recordings of SNr, thalamus, striatum and cerebral cortex, and at 30–63 degrees from vertical at a speed of 10 μm/s until 8 mm below the dura for recordings of cerebellum. They were left to settle for more than 30 min to reduce subsequent drift due to post-insertion brain relaxation. Recording was controlled with Open Ephys software (version 0.5, https://github.com/open-ephys/plugin-GUI/releases) (Siegle, López et al. 2017). Spiking activity and local field potential (LFP) were obtained at 30,000 samples/s and 2,500 sample/s, respectively after 500 Hz high-pass filtering and band-pass filtering with 0.5 – 1kHz range, respectively. We recorded the timing and location of photostimulation at the same time with USB-6001 (National instruments, USA) to align timing of each photostimulation with the neural signals. When the Neuropixel probe was placed to penetrate the cerebellar nuclei, a “bird sign” appeared on the LFP correlation structure (**Fig. 2a**). Histological observation revealed that the presence of this bird mark corresponded to the CN. The wing of the bird would reflect the fact that similar LFP signal appeared from white matter around the CN so that the correlation between the white matters is high, while the CN has specific signal, reducing the correlation between CN and white matter. We finally determined location of each channel at the level of the subdivision within CN or SNr by histological observations.

We recorded neurons from lateral and interposed nucleus of CN. These regions are known to preferentially interact with the motor cortex (Harvey, Porter et al. 1979, Thach, Goodkin et al. 1992, Mushiake and Strick 1993, Ohmae, Kunimatsu et al. 2017). We recorded neurons evenly from the SNr. We focused on the ML axis for the analysis because striato-SNr projection across AP axis seems to be similar (Lee, Wang et al. 2020), and both received the dorsomedial or dorsolateral striatal input where motor cortex sends the projections.

Analysis of electrophysiological data

All analyses were performed with MATLAB (R2020a, Mathworks) or Python (version 3.7). Spike sorting was performed using KiloSort3 (https://github.com/MouseLand/Kilosort). Sorted clusters were manually curated with Phy template GUI (https://github.com/cortex-lab/phy). The spontaneous firing rate of each neuron was obtained by averaging the firing rates for 50 ms before photostimulation.

For the cerebellar recordings, we determined the cell types of the curated neurons in the following way. First, we identified each neuron's region based on the LFP correlation structure described above. In the granule layer, we observed spiking activities with a NAW (negative after wave). Based on

similar descriptions in rodents and monkeys (Van Kan, Gibson et al. 1993, Prsa, Dash et al. 2009, Van Dijck, Van Hulle et al. 2013, Muzzu, Mitolo et al. 2018, Beau, Herzfeld et al. 2024), we classified them as MFs. The complex spike of PCs was classified by a characteristic complex waveform and low firing rate (< 10 Hz) and the simple spike of PCs was identified according to recording location and high firing rate (> 20 Hz) (Cheron, Sausbier et al. 2009, Sedaghat-Nejad, Fakharian et al. 2021, Sedaghat-Nejad, Pi et al. 2022). We did not compare simple and complex spikes from the same neurons because we did not obtain sufficient numbers of PCs with both simple and complex spikes.

To identify "responsive neurons" to cerebral cortex stimulation and "receptive fields" in each responsive neuron, we first extracted the candidate sections that satisfied the following inequalities:

$$\left|\frac{X - mean[bone]}{std[bone]}\right| > 1.64,$$

where X is the mean firing rate of the neuron 0–50 ms after stimulation and [bone] indicates stimulation at the skull surface. Then, we excluded the candidate sections surrounded with ≤ four candidate sections among eight surrounding sections. Finally, if any candidate section was surrounded by ≥ five candidate sections among eight surrounding sections, we defined the neuron and candidate sections as responsive neuron and receptive fields, respectively. This criterion collects stimulated sections that form a local cluster based on the fact that the distance between the sections is smaller than the resolution of the stimulus. Among 10,000 randomly shuffled data, no data satisfied this criterion. We confirmed that it identified fewer neurons than those that were visually identifiable, which allowed us to limit our analysis to neurons that had responded unambiguously.

PSTHs were created by collecting the firing responses to the receptive fields from 50 ms before to 150 ms after photostimulation in each trial. The peak latency was obtained by finding a maximum or minimum value after convolving the PSTH with a Gaussian function with sigma of 3 ms. To examine onset latency, the value of convoluted PSTH at the time of stimulation and its maximum or minimum up to 50 ms after stimulation was standardized to 0 and 1, respectively. The time at which this value first exceeded 0.4 was determined to be the onset latency. To obtain the average responsive maps, we translated each map based on the position of bregma and angle of midline before averaging. K-means clustering was done by the MATLAB function "kmeans". For each pair that was simultaneously recorded, a −50 ms to 50 ms cross-correlation range of spiking activity was calculated, and a significant interaction was defined when the peak was > 99.8% of the peak synchronization level calculated by shuffling spikes in the same window 1000 times. Among them, we visually inspected pair by pair to determine the putative monosynaptic interactions.

Simulation of a spiking neural network

We created a spiking neural network with the Izhikevich model (Izhikevich 2003, Izhikevich 2007) in the Brian2 simulator in Python. The time step was set at 0.1 ms. The Izhikevich model is described as follows:

$$\frac{dv(t)}{dt} = 0.04v(t)^2 + 140 - u(t) + I(t),$$

$$\frac{du(t)}{dt} = a\,(bv(t) - u(t)),$$

where u is potassium channel conductance, v is membrane potential, a is the leak current of the potassium channel, b is the voltage dependence of the potassium channel, c is post-depolarization potential, and d is the opening of the potassium channel after firing. When v exceeded 15 mV, the neuron was regarded to have an action potential, and v and u were reset to c and $u + d$,

respectively. We determined parameters $a, b, c,$ and d based on previous studies (Izhikevich 2007, Thibeault and Srinivasa 2013, Muddapu, Mandali et al. 2019) (**Extended Data Table 2**).

We set the network connectivity of basal ganglia in detail based on recent anatomical studies (Hintiryan, Foster et al. 2016, Foster, Barry et al. 2021, Jeon, Lee et al. 2022) (**Extended Data Fig. 3**). Conversely, although recent studies have provided essential knowledge (Kebschull, Richman et al. 2020, Pisano, Dhanerawala et al. 2021, Wu, Sarpong et al. 2023), because of limited projectome data of the cerebro-cerebellar loop circuit at a subdivision level (for instance, at the level of the microzone (Sugihara, Fujita et al. 2009)), we modeled only a part of the cerebellar network with known anatomical connections. We set the conduction delay of each connection as shown in **Extended Data Fig. 3**. Each synaptic input was delivered immediately after the delay time as a transient voltage step in the Izhikevich model. The simplified diagram combining all the simulated networks is shown in **Fig. 7a**.

As an input from the cerebral cortex, we simulated a Poisson spike train as a spiking activity of association cortex (N = 600 neurons). The spontaneous firing rate was set to 10 Hz, and the firing rate after virtual optogenetic stimulation was set to 100 Hz (5 ms). Virtual optogenetic stimulation was administered 15 times during 3000 ms of stimulation at various intervals. By visualizing a PSTH of each subdivision or each region, we manually modified synaptic weight, connection probability, and conduction delay by referring to electrophysiological data obtained in this study. Note that although we searched a broad set of parameters, the overall connection diagram was not changed, indicating that the circuit is consistent with our anatomical knowledge. After determining the parameters, we ran the simulation for longer time periods (6000 ms including 20 -30 stimulations), which were repeated 5 times.

Reservoir based reinforcement learning model

The dynamics of the cerebral cortex were modeled as a reservoir circuit described as

$$\tau \frac{dx_i}{dt} = -x_i + \sum_{j=1}^{N} W_{ij}^{REC}\, r_j + W_{ij}^{tone} y_{tone} + W_{ij}^{reward} y_{reward} + I_i^{noise},$$

$$z_{HD}(t) = \sum_{i=1}^{N} W_i^{HD} \int_0^{t_0} f_{HD}(t)\, s_i(t-t')\, dt',$$
$$z_{D}(t) = \sum_{i=1}^{N} W_i^{D} \int_0^{t_0} f_{D}(t)\, s_i(t-t')\, dt',$$
$$z_{ID}(t) = \sum_{i=1}^{N} W_i^{ID} \int_0^{t_0} f_{ID}(t)\, s_i(t-t')\, dt',$$
$$z_{P1}(t) = \sum_{i=1}^{N} W_i^{P1} \int_0^{t_0} f_{P1}(t)\, s_i(t-t')\, dt',$$
$$z_{P2}(t) = \sum_{i=1}^{N} W_i^{P2} \int_0^{t_0} f_{P2}(t)\, s_i(t-t')\, dt',$$
$$z_{P3}(t) = \sum_{i=1}^{N} W_i^{P3} \int_0^{t_0} f_{P3}(t)\, s_i(t-t')\, dt',$$

where $r_i = tanh(x_i)$ represents the firing rate of the *i-th* recurrent unit $(i = 1, \ldots, N)$, $s_i = (r_i + 1)^2$, and the filter functions f_{HD}, f_D, f_{ID}, f_{P1}, f_{P2}, f_{P3} were defined by the double-exponential function fitted to the experimental data (**Fig. 8b**). The reservoir network was simulated at the time step of 1 ms. The variable y_{tone} and y_{reward} represents the input of tone and reward, respectively (1 or 0). $N = 800$ is the number of units, and $\tau = 20\, ms$ is the unit time constant. The recurrent connectivity is represented by the $N \times N$ sparce matrix W_{ij}^{REC} where the connection probability between units is $p = 0.14,$ and the weight follows a Gaussian distribution with a mean of zero and a standard deviation of 0.189. The activity of the network was read out by z_{HD}, z_D, z_{ID}, z_{P1}, z_{P2}, and z_{P3} through the $1 \times N$ output connectivity matrix W_i^{HD}, W_i^{D}, W_i^{ID}, W_i^{P1}, W_i^{P2}, W_i^{P3}, with initial values determined by a Gaussian distribution with a mean of zero and a standard deviation of 0.02. Here, because we regarded phase 3 as a rebound of phase 2, W_i^{P3} was the same

as W_i^{P2}. The input weight vectors W_{ij}^{tone} and W_{ij}^{reward} followed a Gaussian distribution with a mean of zero and a standard deviation of 5. The values of y_{tone} and y_{reward} were 0, except during a tone or reward, comprising a step with a duration of 50 ms and amplitude of 1. A noise current was included as a $N \times 1$ random vector, I_i^{noise}, defined with a Gaussian distribution with a mean of zero and a standard deviation of 0.001.

Reinforcement learning task

The agent received the tone cue and reward as inputs and determined whether to hold or pull the lever at each time step of 100 ms. When the agent held the lever for 1 s, the tone cue was presented. If the agent pulled the lever before holding the lever for 1s, the tone cue was not presented, and the agent needed to hold the lever for 1s for the next tone cue. The agent needed to pull the lever within 0.3 s after tone cue presentation to get the reward. If the agent did not pull the lever within 0.3 s, the agent did not get the reward and needed to hold the lever for 1 s to receive the next tone cue. We have shown that rats can learn this task quickly (within a day of training) (Kimura, Saiki et al. 2012, Kimura, Saiki et al. 2017, Saiki, Sakai et al. 2018, Kawabata, Soma et al. 2020, Yoshizawa, Miyamura et al. 2023).

The agent determined whether to pull or hold the lever every 100 ms, by comparing the pull value (q_{pull}) and hold value (q_{hold}). We defined these values as follows:

$$q_{pull} = z_D + z_{P1} + z_{P3} \ ,$$

$$q_{hold} = z_{HD} + z_{ID} + z_{P2} \ .$$

Here, the excitatory and inhibitory effect on the thalamus was regarded as the pull value and hold value, respectively. If the sum of these activities integrated in M1 from the thalamus or in the brainstem circuits exceeded the motor threshold, the lever was pulled. Thus, with q_{pull} and q_{hold}, we defined the probability of pulling, P_{pull}, as follows:

$$P_{pull} = \left[\frac{1}{1 + \ exp\,(\beta\, q_{hold} - \ \beta\, q_{pull})} - cost\right],$$

where $[x]$ returns x if x is positive and 0 if x is zero or negative, β = 1.2 is inverse temperature, and cost = 0.45 is the bias parameter. Every 100 ms, the maximum value of this probability was calculated, and this value determined pull or hold. A pull at the appropriate time was rewarded; however, there was a time lag of 0.2 s between the decision to output the action and the reward. This time lag was broadly consistent with the experimental data.

Learning

This simple model assumed that synaptic plasticity does not occur within the reservoir but only affects the direct pathways and PFs. All the synaptic plasticity was based on RPE, δ_t, defined as follows:

$$\delta_t = reward(t) + \gamma Q - Q' \,,$$

where the discount rate γ was set to a half-life of 3 s. Q and Q' are values of consecutive time steps as follows:

$$Q = q_{pull}\,(t) - \ q_{pull}(t),$$

$$Q' = q_{pull}\,(t+1) - \ q_{pull}(t+1).$$

Synaptic weight was renewed every 1 s (10 behavioral steps). Under the default condition, synaptic changes were made to the direct pathway and phase 2 as follows:

$$dw_D = \alpha\, \delta_t\, z_D \,,$$

$$dw_{P2} = -\,\alpha\, \delta_t\, z_{P2} \,,$$

where the learning rate was $\alpha = 0.0025$. Additionally, random synaptic fluctuations with a standard deviation of 0.001 were added, and each synaptic weight was divided by the sum of synaptic weights in the corresponding pathways according to homeostatic plasticity.

Synaptic changes in the direct pathway and PF-PC pathway in the cerebellum correspond to the dopamine-dependent LTP in the corticostriatal synapse (Yagishita, Hayashi-Takagi et al. 2014) and CF-dependent LTD in the PF-PC synapse, respectively, when RPE is positive. Negative RPE increases local ACh concentration (Chantranupong, Beron et al. 2023), and cholinergic input induces LTD in the D1-positive medium spiny neuron (Shen, Plotkin et al. 2015). PF-PC synapses undergo LTP when PCs only exhibit simple spikes without complex spikes (Hirano 1990). Accordingly, we allow for bidirectional plasticity in both direct and PF-PC pathways.

Statistics

The Wilcoxon's rank-sum test and χ^2- test were used for pairwise comparisons. Data were expressed as mean ± S.E.M unless noted otherwise.

Figures

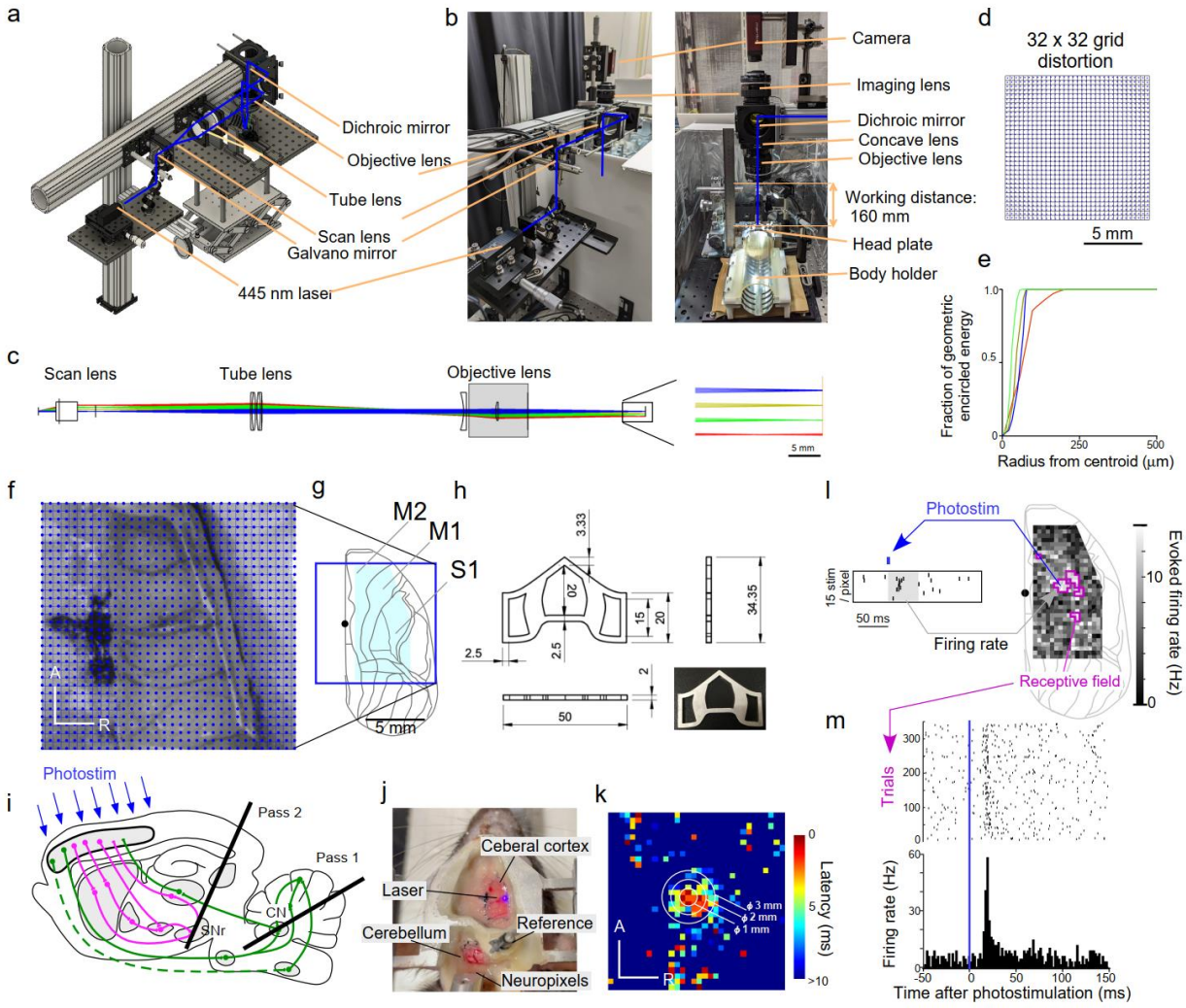

Figure 1. Optogenetic stimulation and electrophysiological recordings.
a. 3D CAD data for the system. **b.** Photographs of the system. WD, working distance. **c.** Four laser beams correspond to scanning angles of 0, 4, 8, and 12 degrees, which focus at distances of 0, 2.4, 4.7, and 7.1 mm from the center, respectively. The objective lens (Nikon camera lens) was substituted by a lens with the same focal length. **d.** Grid distortion of 32 × 32 stimulation points (10 mm × 10 mm). **e.** Proportion of encircled energy as a function of the distance from the centroid. **f.** A photograph of thinned skull preparation. The blue point corresponds to each point of photostimulation. **g.** Dorsal view of brain atlas of right hemisphere. The blue square represents the 10 mm × 10 mm stimulation area. The black dot denotes the bregma. **h.** Headplate design. **i.** Approximate positions of recording pass 1 (for cerebellar nuclei (CN)) and recording pass 2 (for substantia nigra pars reticulata (SNr)). **j.** A photograph from the top during photostimulation of the cerebral cortex and recording at the cerebellum. **k.** Spike latency map of a single neuron in the cerebral cortex showing the resolution of photostimulation. **l.** A representative responsive map for a single CN neuron. The purple rectangle indicates the receptive field of the neuron. **m**. A raster plot (top) and PSTH (bottom) for trials in which photostimulation was performed on the receptive field in **l.**

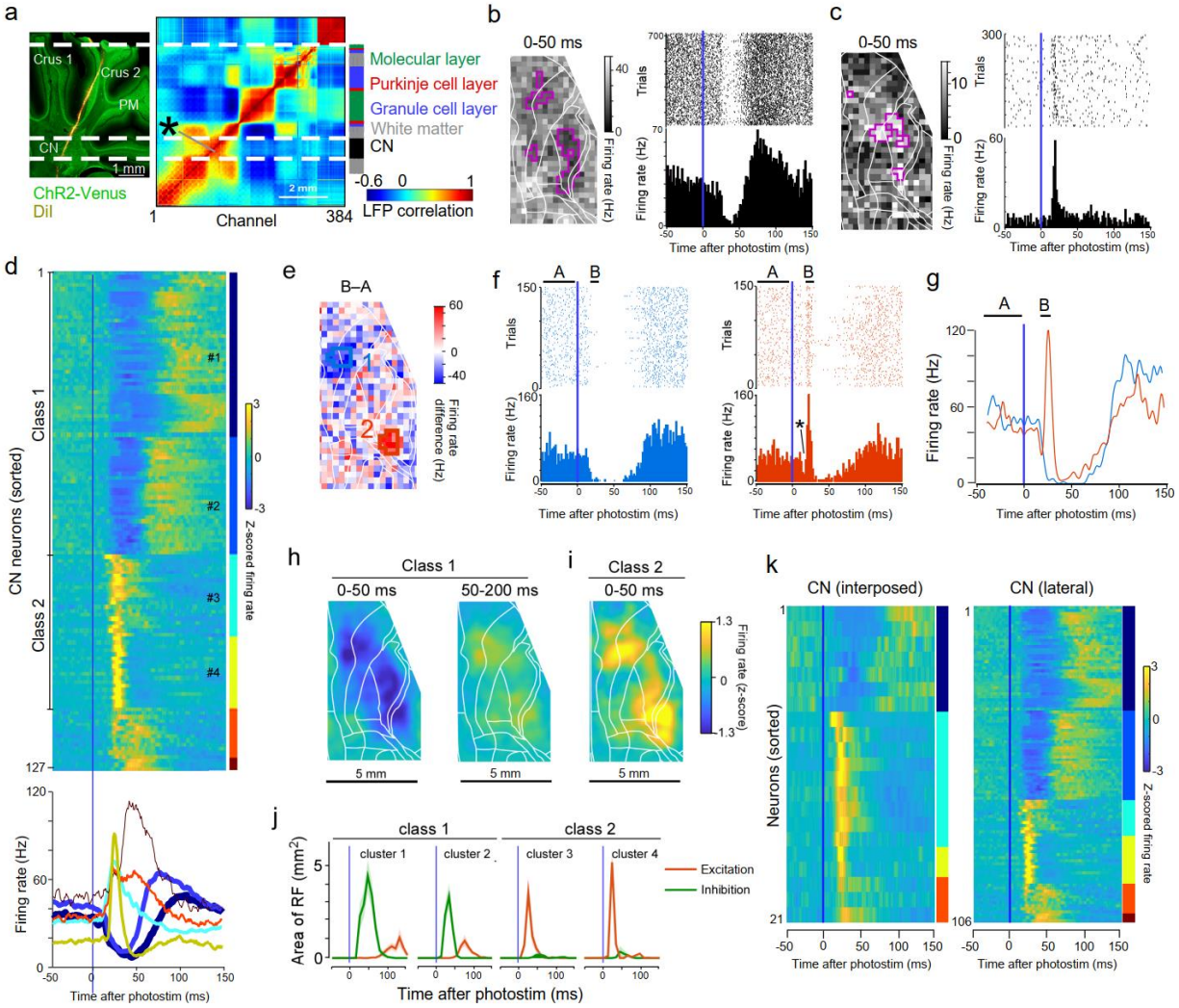

Figure 2. Two major classes of response patterns observed in cerebellar nuclei (CN) neurons.

a. A sagittal section of cerebellum in a ChR2-Venus transgenic rat (left) and local field potential (LFP) correlation structure of the corresponding animal recorded with Neuropixels (right). DiI fluorescence shows electrode location. Dotted lines indicating boundaries of LFP correlation structure correspond to histologically confirmed cerebellar layer structure and cerebellar nuclei. **b,c.** Response maps of typical class 1 (**b**) and 2 (**c**) responses in CN (left). Magenta frames indicate responsive pixels. Raster plots and PSTHs for the responsive pixels (right). **d.** Z-scored PSTH of all CN neurons clustered by K-means clustering (top) and mean PSTH of each cluster (bottom). Colors correspond to cluster numbers. The thickness indicates the numbers of neurons in the cluster. **e.** A map of the difference in firing rate at two time bins: −50–0 ms (A) and 20–30 ms (B) after stimulation of a CN neuron. **f.** Raster plots and PSTHs for the blue and red polygons in **e**. * indicates a transient inhibitory response before the fast excitatory response. **g.** An overlay of the PSTHs in **f**. **h.** Average input maps of class 1 neurons at 0–50 ms (left) and 50–200 ms (right) in CN. **i.** An average input map of a class 2 neuron in CN. **j.** Time course of excitatory and inhibitory responsive areas in clusters #1–4. **k**. The same analysis as **d**, but separated according to recording location.

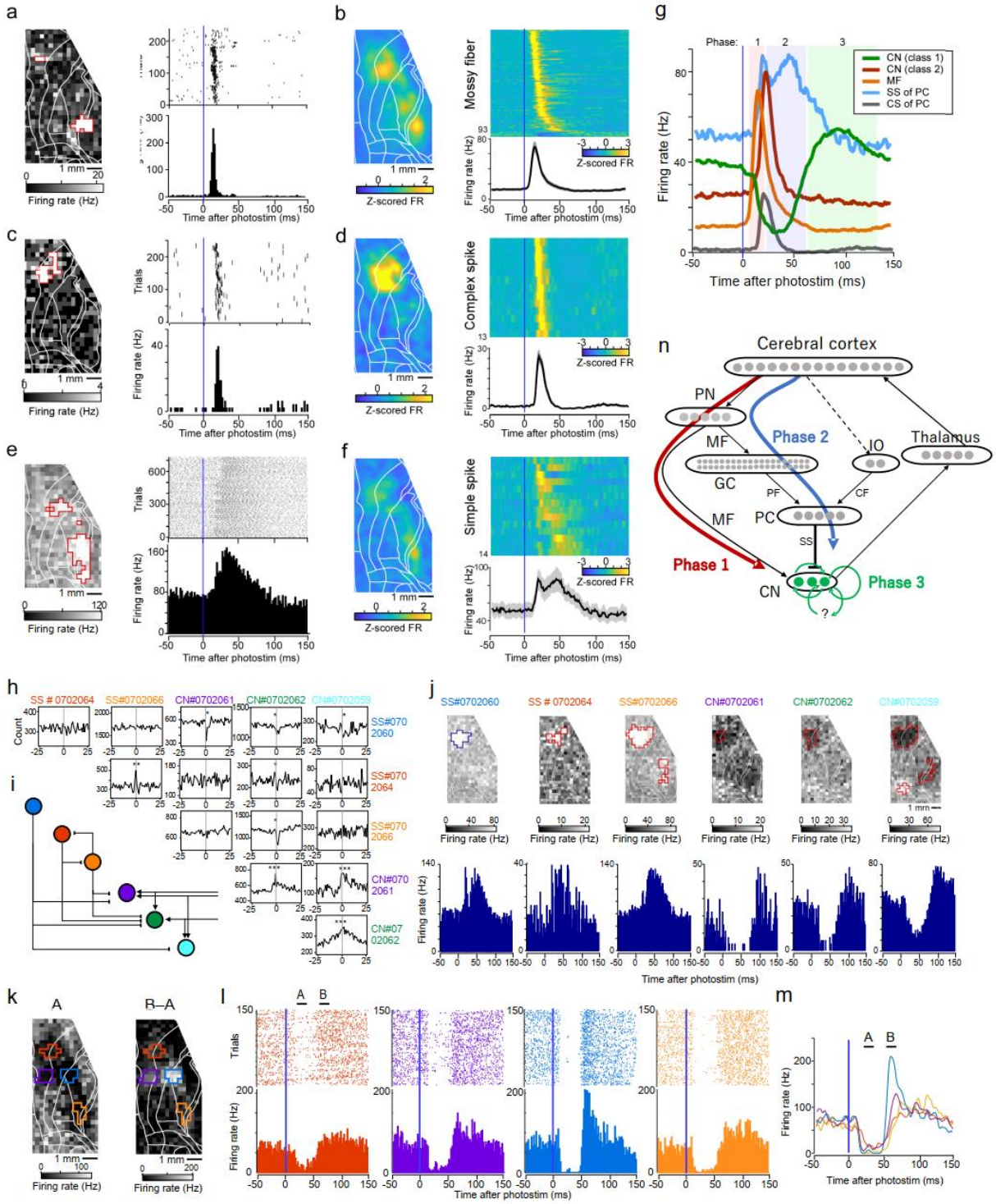

Figure 3. Activity propagation from the cerebral cortex to cerebellar nuclei (CN) neurons.

a,c,e. A response map, raster plot, and PSTH of a mossy fiber (MF) neuron (**a**) and complex spike (**c**) and simple spike (**e**) of a PC. **b,d,f.** Normalized average responses (left) of MF neurons (**b**) and complex spikes (**d**) and simple spikes (**f**) of PCs. The order was sorted by the peak time. Average maps of all activities (right). **g.** Mean firing rates of CN neurons with class 1 responses, CN neurons with class 2 responses, MFs, SS (simple spike), and CS (complex spike). Shaded areas indicate phases 1–3. **h.** Cross-correlogram of simultaneous recordings of three PCs (SS) and three neurons in CN. **i.** A predicted synaptic circuit among neurons in **h. j.** Response maps and PSTHs of six neurons shown in **h**. All PSTHs were generated in trials with photostimulation of the receptive field of the blue neuron (SS#0702060) for comparison.

k. Firing rates 20–40 ms after photostimulation (A in **l**) of a CN neuron (left) are shown as a map. Firing rates 50–70 ms after photostimulation (B in **l**) minus that of A of the same neuron are shown as a map (right). **l.** Raster plots and PSTHs of CN neurons from the color-corresponding areas specified in **k. m.** Mean firing rates of CN neurons from the color-corresponding areas in **k** when photostimulated**. n.** Possible pathways from the cerebral cortex to CN. Phases 1, 2, and 3 correspond to the time for excitatory input in class 1 response, inhibitory input in class 2 response, and excitatory input in class 2 response.

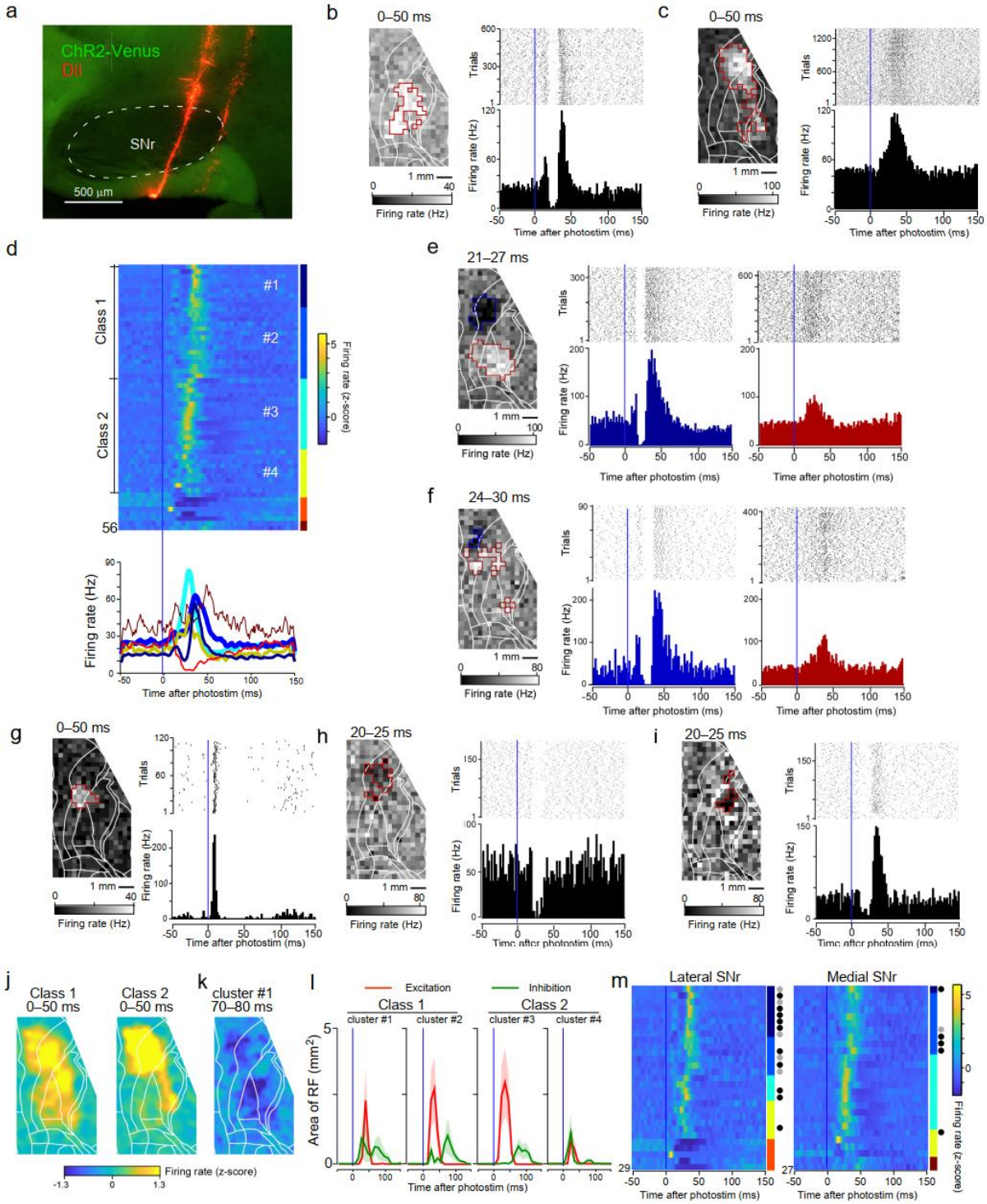

Figure 4. Analysis of single neuron response patterns of substantia nigra pars reticulata (SNr) to cortical stimulation. **a.** A sagittal section showing electrode traces with DiI. **b.** A map, raster plot, and PSTH of a typical SNr neuron with class 1 response (a triphasic response). **c.** A typical neuron with class 2 response (monophasic excitatory response). **d.** Z-scored PSTH of all responsive SNr neurons clustered by K-means clustering (top) and the mean PSTH of each cluster (bottom). Colors correspond to cluster numbers. The thickness indicates the numbers of neurons in the cluster. **e,f.** Examples of SNr neurons that were classified as class 1 but also received class-2-like monophasic excitatory input. **g,h,i**. Neurons showing a very fast excitatory monophasic response (**g**), monophasic inhibitory response (**h**), and inhibition-excitation pattern (**i**). **j.** Average input maps of neurons with class 1 (left) and class 2 (right) responses in SNr.

k. An inhibitory response map of cluster #1 neurons in SNr. **l.** Time courses of the responsive areas. **m.** The same analysis as **d**, but separated according to recording location. Black and gray circles indicate triphasic and inhibition-excitation patterns, respectively.

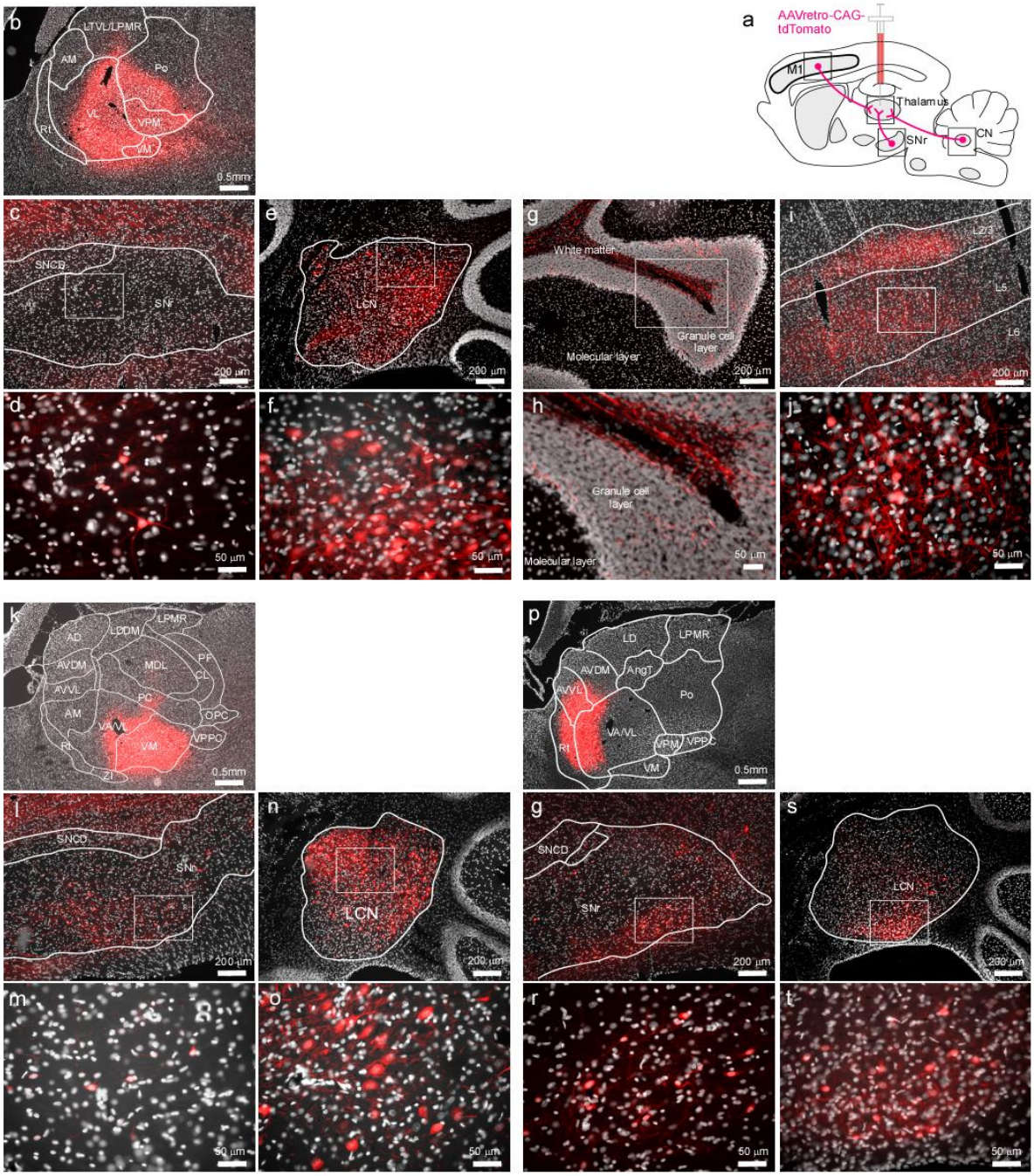

Figure 5. A retrograde tracer revealing thalamic projections from substantia nigra pars reticulata (SNr) and cerebellar nuclei (CN).

a. Schematic of tracer experiments. **b.** Sagittal section 2 weeks after injection of AAVretro-CAG-tdTomato into the VL nucleus of thalamus. White is DAPI fluorescence showing localization of DNA. **c.** The tdTomato fluorescence around the ipsilateral SNr. **d.** Expanded image corresponding to the rectangle in **c. e.** The tdTomato fluorescence around the contralateral CN (LCN, lateral cerebellar nucleus). **f.** Expanded image corresponding to the rectangle in **e. g.** Axon collateral of CN neurons into the cerebral granule cell layer. **h.** Expanded image corresponding to the rectangle in **g. i.** The tdTomato fluorescence around the ipsilateral motor cortex. **j.** Expanded image corresponding to the rectangle in top panel. **k-o.** The same images as **b-f** of an injection experiment to the VM nucleus of thalamus. **p-t.** The same images as **b-f** of an injection experiment to the VA nucleus of thalamus.

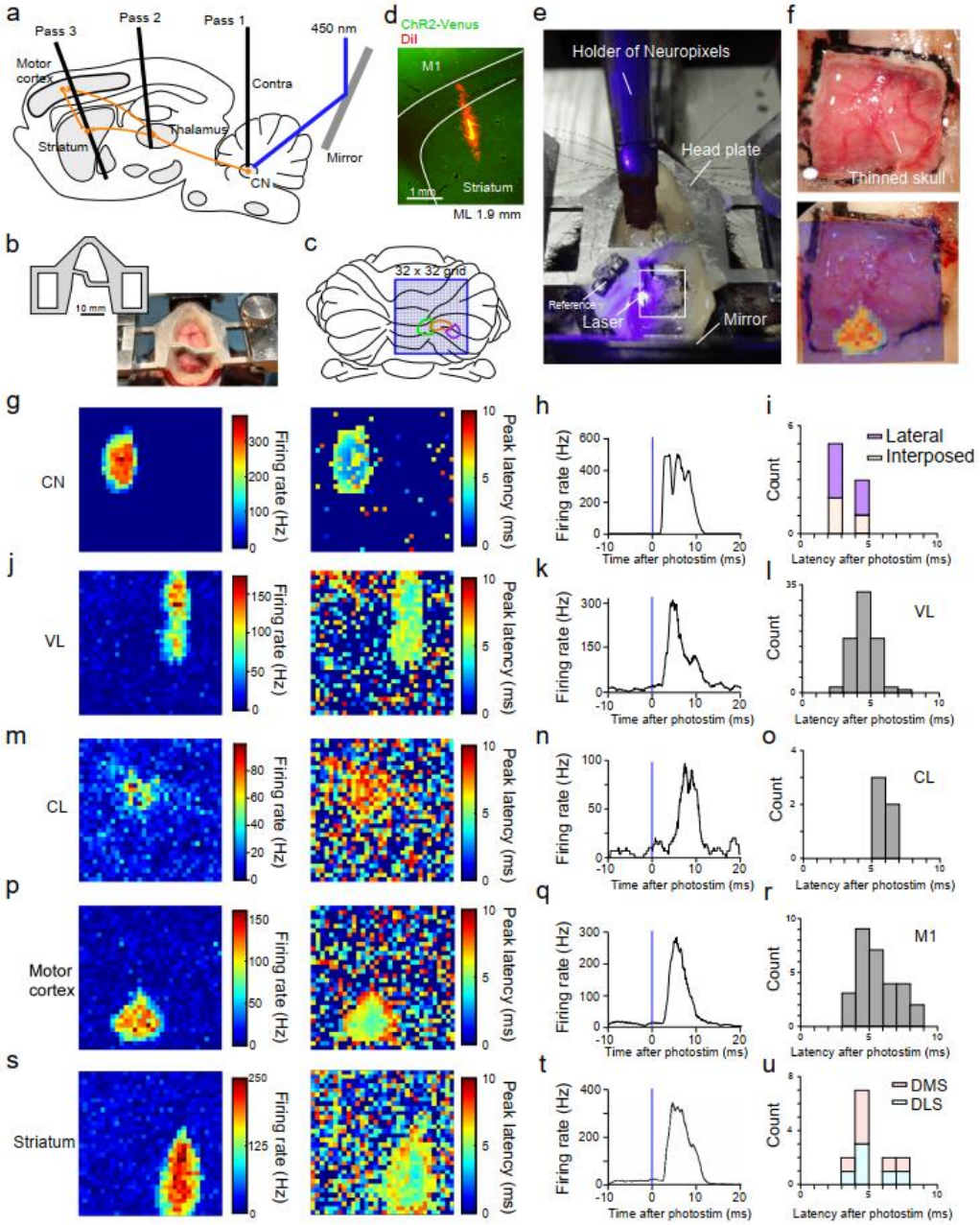

Figure 6. Activity propagation from the cerebellum to the striatum.
a. Approximate positions of recording pass 1 for CN, pass 2 for the thalamus, and pass 3 for the motor cortex and striatum. The mirror was positioned behind the cerebellum to direct the laser to CN. **b.** A headplate optimized for this experiment. **c.** The cerebellum viewed from the angle of laser incidence. The blue frame indicates the photostimulation area. The approximate position of the lateral (purple), interposed (orange), and medial (green) nucleus were overlayed. **d.** Representative fluorescence image used to identify the location of the recording electrode. **e.** A photograph during photostimulation of the cerebellum and recording at the contralateral cerebral cortex. **f.** A photograph of transparent skull on the cerebellum (top). A response map was overlayed (bottom). **g.** Response map (left) and map of the peak latency (right) of a neuron recorded in interposed CN. **h.** The PSTHs of the receptive fields. **i.** Latency histograms of all neurons recorded in CNs. **j-l.** The same analysis as **g-i** for neurons in VL. **m-o.** The same analysis as **g-i** for neurons in CL. **p-r.** The same analysis as **g-i** for neurons in motor cortex. **s-u.** The same analysis as **g-i** for neurons in striatum.

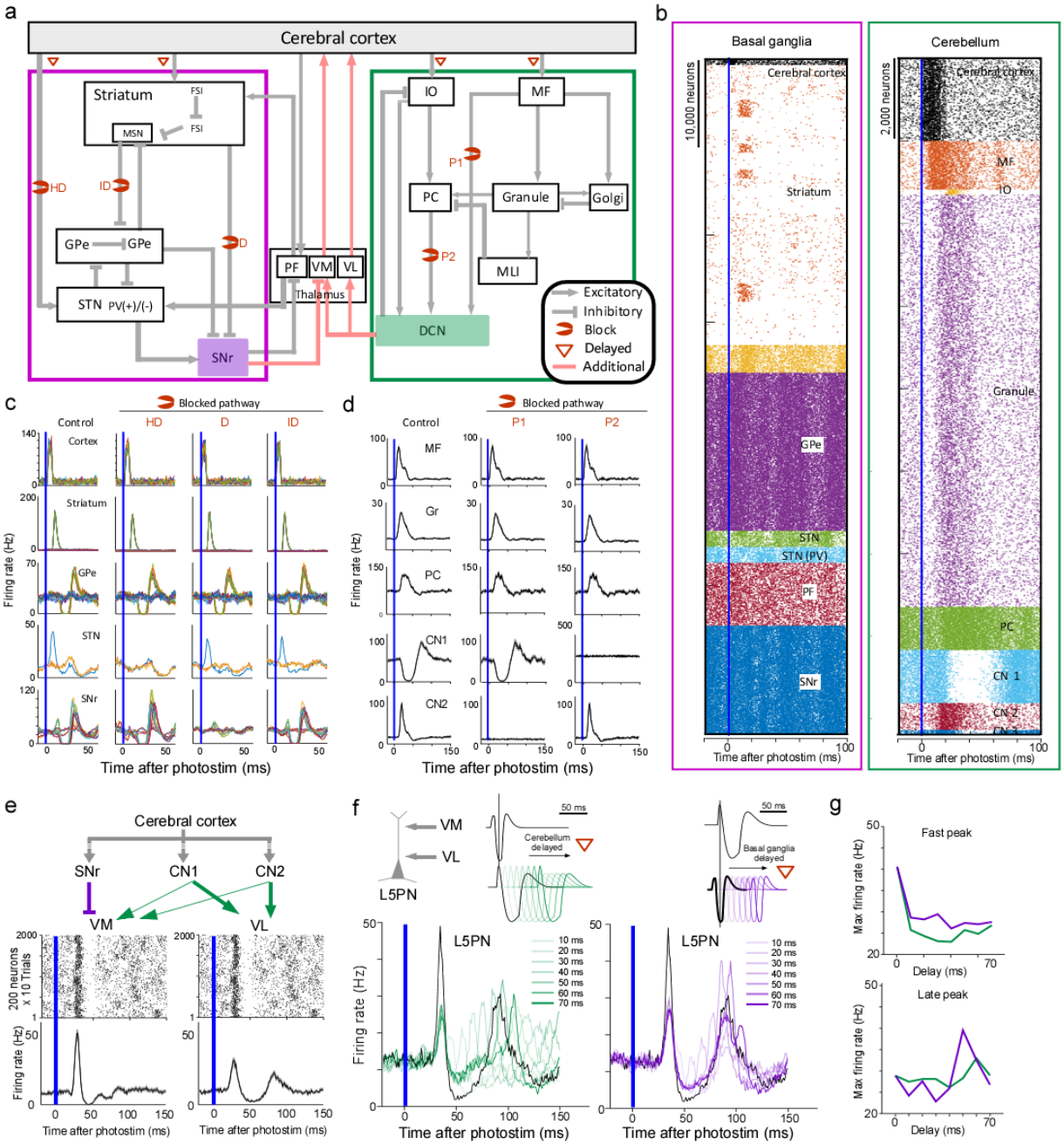

Figure 7. Simulation of spiking neurons based on the connectome data.

a. Circuit schematic of the basal ganglia and cerebellum (see also **Extended Data Fig. 3a**). In the basal ganglia, submodule-level details were constructed based on connectome data (**Extended Data Fig. 3b**). Both share input from the cerebral cortex and output to the thalamus. **b.** Raster plot of simulated neurons before and after stimulation (single trial). **c.** PSTHs of major neurons in the basal ganglia under control conditions and after blocking the hyperdirect, direct, and indirect pathways. Colors indicate submodules. **d.** PSTHs of major neurons in the cerebellum under control conditions and after blocking MF-CN synapses (P1) and PC-CN synapses (P2). **e.** Simplified circuit for the simulation of VM and VL (top). Raster plots and PSTHs of VM and VL neurons (bottom). **f.** L5PN was assumed to receive both inputs from VM and VL (top left). The firing rate of L5PN was simulated when the signal from cerebellum was delayed (left), or when the signal from basal ganglia was delayed (right). **g.** Maximum firing rate of the L5PN at the fast peak (<50 ms) as a function of the delay-time of basal ganglia (purple) and cerebellum (green) (top). The same analysis for the late peak (>50 ms) (bottom)**.**

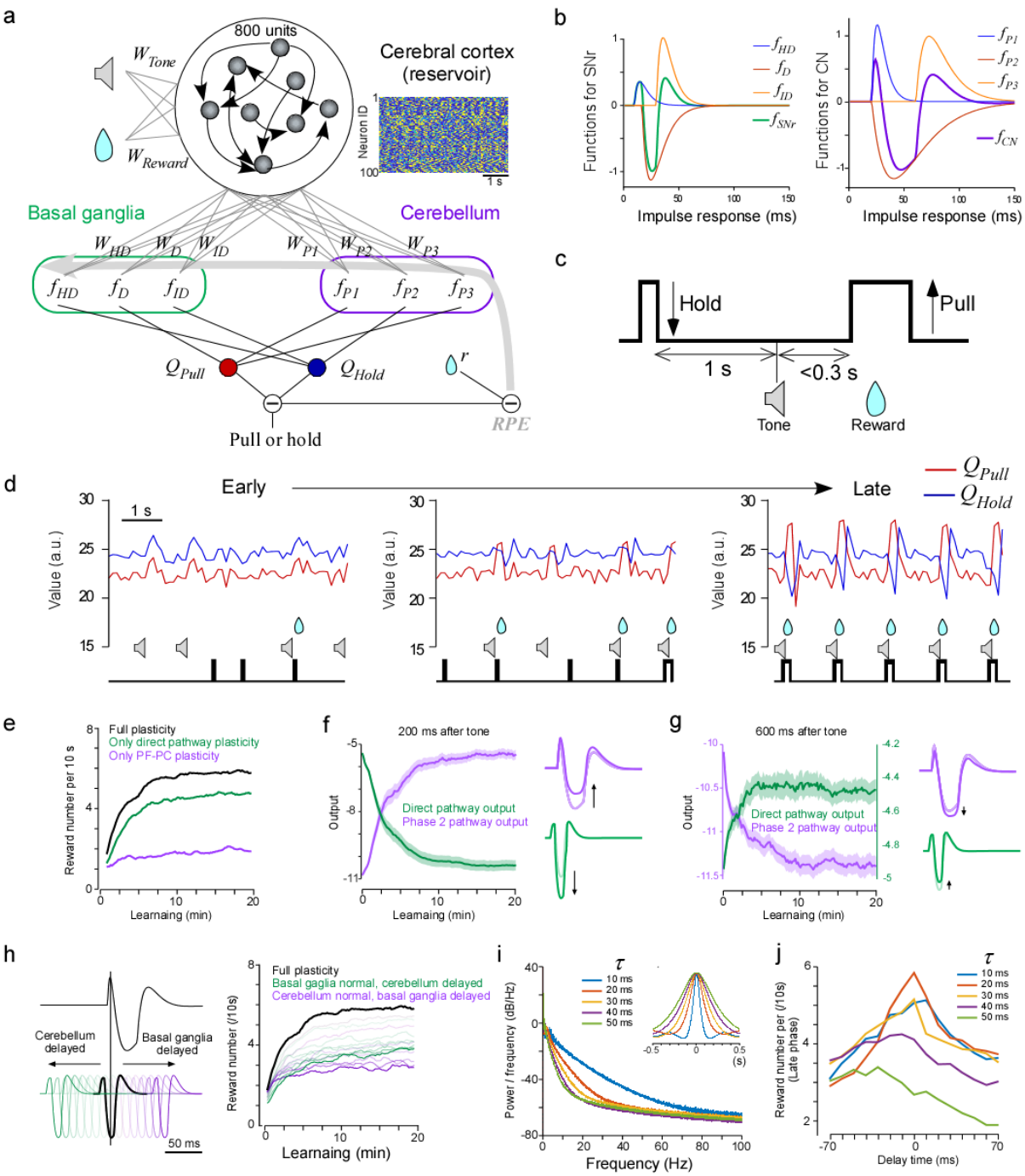

Figure 8. Reservoir-reinforced learning model of the cortex, cerebellum, and basal ganglia.

a. The task structure. The agent is rewarded for holding the lever for 1 s followed by a sound cue and pulling the lever within 0.3 s. **b.** Double-exponential curves mimicking substantia nigra pars reticulata (SNr) (left) and cerebellar nuclei (CN) (right) activity. **c.** Schematic of the model. Cerebral cortex activity was simulated by a reservoir circuit that receives sound and reward inputs. The basal ganglia and cerebellum each integrate three synaptic strengths and three functions, each of which mimic the experimental data. The output from basal ganglia and cerebellum finally combined to a pull value and hold value. The difference between these values determined pull or hold once in 100 ms. Synaptic plasticity was induced by RPE. **d.** Examples of 6 s time series, pull or hold values, movement outputs, sound cues, and rewards in early to late learning stages. **e.** Learning curves under control conditions and after blocking synaptic plasticity in basal ganglia or cerebellum. **f.** Time course of direct pathway output (green) and P1 pathway output (purple) at 200 ms after tone presentation during learning. **g.** The same analysis as in f, but 600 ms after tone presentation. **h.**

Schematic of signal delay(left). Changes in learning curves after delaying the conduction of corticostriatal or corticopontine projections. A 10 ms delay slowed the learning rate. **i.** Power spectrum of simulated cortical activity when the time constat was changed from 10 – 50 ms. **j.** Timescale of cortical neural activity indicated by colors affects the conduction-delay dependency of learning.

Extended Data Figures

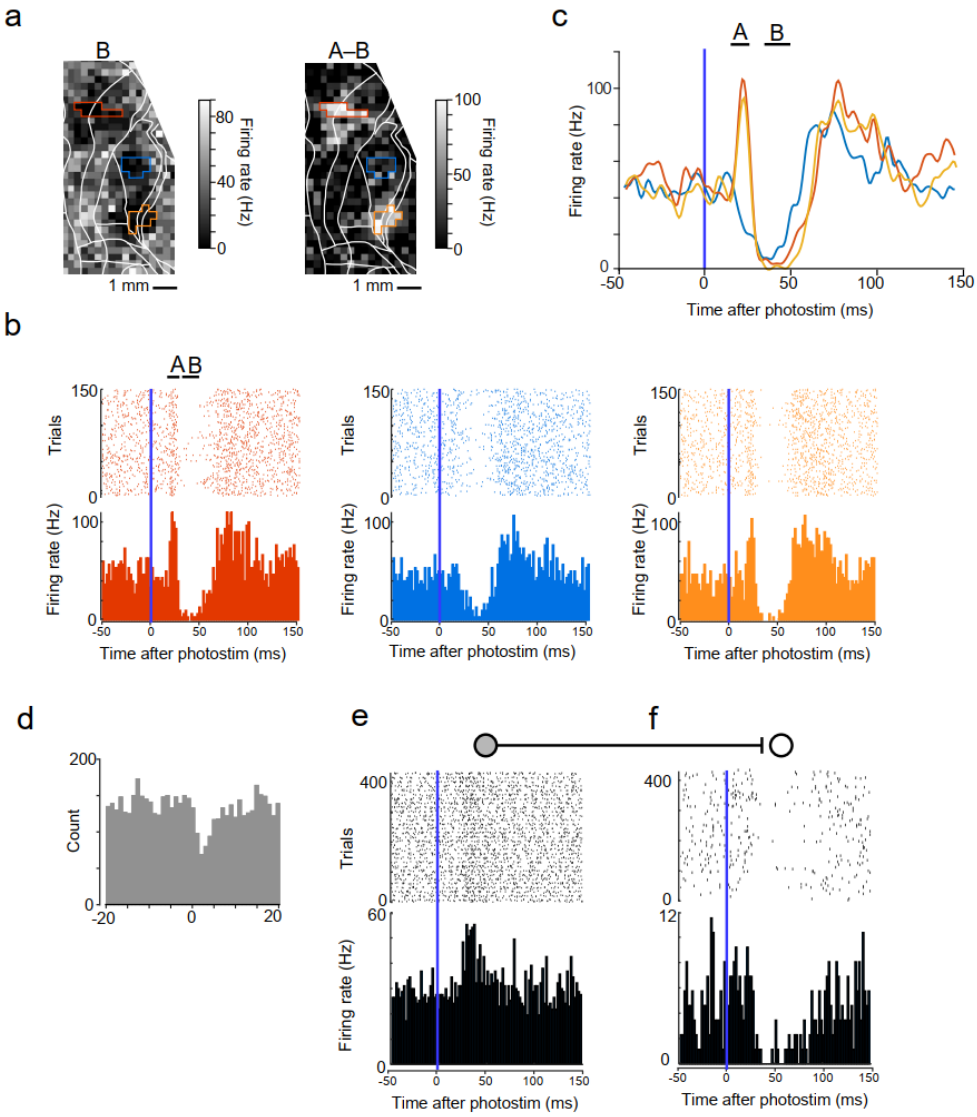

Extended Data Figure 1. Cerebellar nuclei (CN) neuron responses.

a. Maps of firing rates 30–50 ms (B) after stimulation (left) and the difference in firing rates (right) at two time bins: 20–30 ms (A) and 30–50 ms (B). **b.** Raster plots and PSTHs for the stimulus points enclosed by the red, blue, and orange polygons in **a**. **c.** Overlaid PSTHs**. d.** Cross-correlogram of simultaneous recordings of a PC (SS) and a neuron in CN. **e.** Rater plot and PSTH of the presynaptic PC (SS) in **d. f.** Rater plot and PSTH of the postsynaptic CN neuron in **d.** PSTHs in **e** and **f** were generated in trials with photostimulation of the receptive field of the PC for comparison.

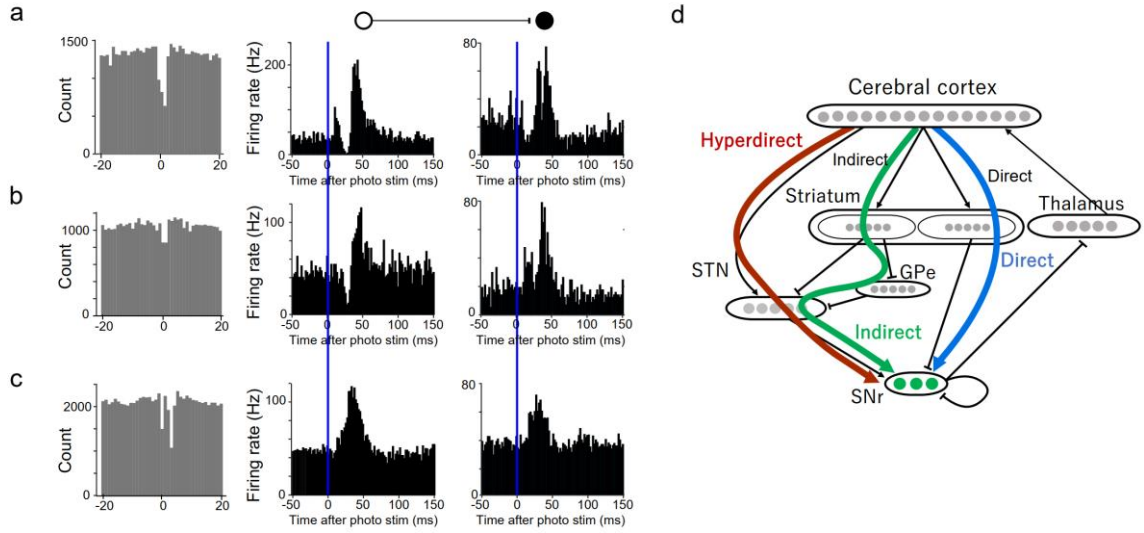

Extended Data Figure 2. Hyperdirect, direct, and indirect pathways are explained by basal ganglia, not by synaptic interaction within the SNr. **a.** An example of cross-correlogram showing inhibitory interaction between simultaneously recorded pair of SNr neurons. The synaptic interaction does not explain the PSTHs. The PSTHs were obtained with the responsive pixels that shared by the two neurons. **b,c.** Examples of the other SNr neuron pairs. **d.** Schematic of the hyperdirect, direct, and indirect pathways.

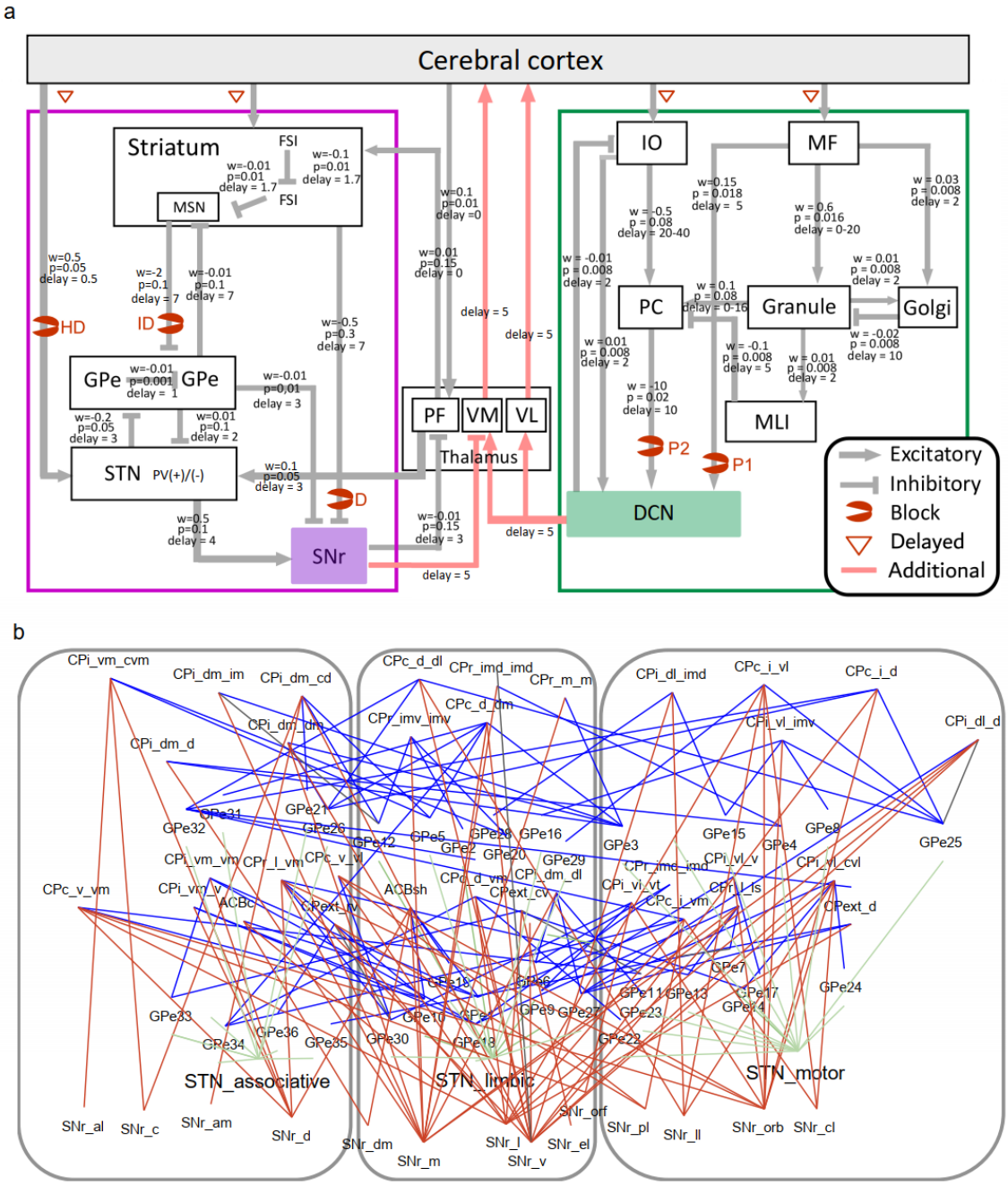

Extended Data Figure 3. The network of cerebral cortex, cerebellum, and basal ganglia. **a.** A circuit diagram with parameters (w: weight in mV, p: probability, and delay in ms). **b.** Based on anatomical data, we constructed a detailed circuit consisting of 16 modules of striatum, 36 modules of external globus pallidus, 3 modules of subthalamic nucleus, and 14 modules of substantia nigra pars reticulata. Each line indicates a connection between subdivisions. The three rectangular frames indicate known clusters (Foster, Barry et al. 2021). Connections among CP (or ACB) (caudate putamen or nucleus accumbens, total 16 clusters), GPe (36 clusters), STN (3 clusters), SNr (14 clusters) were determined according to (Foster et al. 2021, Jeon et al. 2022, Hintiryan et al. 2016). Line colors indicate connection types.

Extended Data Tables

#		Type	Comment	Radius	Thickness	Material	Semi-Diameter	Mech Semi-Dia
0	OBJECT	STANDARD		Infinity	Infinity		0.000	0.000
1		STANDARD		Infinity	0.000		5.500	5.500
2	STOP	STANDARD		Infinity	0.000		0.500	0.500
3		STANDARD		Infinity	24.750		5.500	5.500
4		STANDARD		Infinity	4.250		10.761	10.761
5		STANDARD	Mounting surface	Infinity	-4		17.000	17.000
6	(aper)	BLACKBOX	LSM03-VIS.ZBB	Infinity	29.935		12.700	12.700
7		STANDARD	Last mech surface	Infinity	25.150		8.621	8.621
8		STANDARD		Infinity	215.000		8.134	8.134
9	(aper)	STANDARD		760.00	2.000	SF2	25.400	25.400
10	(aper)	STANDARD		186.80	5.000	N-BK7	25.400	25.400
11	(aper)	STANDARD	AC508-400-A	-219.80	0.000		25.400	25.400
12		STANDARD		Infinity	2.000		15.700	15.700
13	(aper)	STANDARD	AC508-400-A	219.80	5.000	N-BK7	25.400	25.400
14	(aper)	STANDARD		-186.80	2.000	SF2	25.400	25.400
15	(aper)	STANDARD		-760.00	0.000		25.400	25.400
16		STANDARD		Infinity	280.000		15.499	15.499
17	(aper)	STANDARD	LC1611-A	-77.19	4.000	N-BK7	25.400	25.400
18	(aper)	STANDARD		Infinity	0.000		25.400	25.400
19		STANDARD		Infinity	41.000		11.193	11.193
20	(aper)	STANDARD	KPX385	54.47	3.400	BK7	12.500	12.500
21	(aper)	STANDARD		Infinity	41.000		12.500	12.500
22		STANDARD		Infinity	0.000		13.982	13.982
23		STANDARD		Infinity	163.483		25.400	25.400
24	IMAGE	STANDARD		Infinity	0.000		7.004	7.004

Extended Data Table 1. A lens data list of the scanning optogenetics system. Shaded areas highlight substitutes of the Nikon camera lens with f = 105 mm.

Region	Cell type	No. of neurons	No. of domains	Spont. firing rate (Hz)	a	b	c	d
Basal ganglia	FSI	3200	32	28 (Berke, Okatan et al. 2004, Gage, Stoetzner et al. 2010)	0.1	0.2	-65	2
Basal ganglia	MSN	32000	32	7 (Miller, Walker et al. 2008)	0.02	0.2	-65	8
Basal ganglia	GPe	18000	36	24 (Mallet, Pogosyan et al. 2008)	0.02	0.2	-65	8
Basal ganglia	STN	3600	6	14 (Yasoshima, Kai et al. 2005, Mallet, Pogosyan et al. 2008)	0.02	0.2	-65	8
Basal ganglia	SNr / GPi	12600	14	32 (Maurice, Thierry et al. 2003)	0.02	0.2	-65	8
Cerebellum	ST	3510	1	20 (Jelitai, Puggioni et al. 2016)	0.1	0.2	-65	2
Cerebellum	BA	910	1	20 (Jelitai, Puggioni et al. 2016)	0.1	0.2	-65	2
Cerebellum	GO	650	1	18 (Muzzu, Mitolo et al. 2018)	0.1	0.2	-65	2
Cerebellum	GR	10000	1	5 (Jelitai, Puggioni et al. 2016)	0.2	0.2	-65	0.05
Cerebellum	PC	1040	1	68 (Jelitai, Puggioni et al. 2016, Muzzu, Mitolo et al. 2018)	0.02	0.2	-65	0.01
Cerebellum	IO	130	1	1 (Jelitai, Puggioni et al. 2016)	0.1	0.2	-65	2
Cerebellum	MF	1170	1	15 (Muzzu, Mitolo et al. 2018)	0.2	0.2	-65	0.05
Cerebellum	DCN	2150	2	50 (this study)	0.02	0.25	-65	0.05
Thalamus	PF	7200	6	8 (Marlinski and Beloozerova 2014, Urbain, Salin et al. 2015)	0.02	0.25	-65	0.05
Thalamus	VM	200	1	8 (Marlinski and Beloozerova 2014, Urbain, Salin et al. 2015)	0.02	0.25	-65	0.05
Thalamus	VL	200	1	8 (Marlinski and Beloozerova 2014, Urbain, Salin et al. 2015)	0.02	0.25	-65	0.05
Cerebral cortex	L5PN	200	1	12 (O'Connor, Peron et al. 2010)	0.02	0.2	-65	8

Extended Data Table 2. The numbers of neurons, numbers of domains, spontaneous firing rate, and four parameters of the Izhikevich model. FSI: fast spiking interneuron, MSN: medium spiny neuron, GPe: external segment of global pallidus, STN: subthalamic nucleus, SNr: substantia nigra pars reticulata, GPi: internal segment of global pallidus, ST: stellate cell, BA: basket cell, GO: Golgi cell, GR: granule cell, PC: Purkinje cell, IO: inferior olive cell, MF: mossy fiber, DCN: deep cerebellar nucleus, VM: ventromedial nucleus, VL: ventrolateral nucleus. L5PN; layer 5 pyramidal

991 neuron. The number of neurons in each type in basal ganglia, cerebellum, and PF were determined by the single-cell-
992 resolution whole-brain atlas (Murakami, Mano et al. 2018).
993

Supplementary information

The code of the spiking neural network, code of reservoir model, CAD files of the headplate, parts list, Zemax files for the scan-optogenetics system will be made available upon publication. Electrophysiological data is available upon request.

References

Aizenman, C. D. and D. J. Linden (1999). "Regulation of the rebound depolarization and spontaneous firing patterns of deep nuclear neurons in slices of rat cerebellum." Journal of neurophysiology **82**(4): 1697-1709.

Alexander, G. E. and M. D. Crutcher (1990). "Functional architecture of basal ganglia circuits: neural substrates of parallel processing." Trends in neurosciences **13**(7): 266-271.

Alexander, G. E., M. R. DeLong and P. L. Strick (1986). "Parallel organization of functionally segregated circuits linking basal ganglia and cortex." Annual review of neuroscience **9**(1): 357-381.

Allen, G. and N. Tsukahara (1974). "Cerebrocerebellar communication systems." Physiological Reviews **54**(4): 957-1006.

Beau, M., D. J. Herzfeld, F. Naveros, M. E. Hemelt, F. D'Agostino, M. Oostland, A. Sánchez-López, Y. Y. Chung, M. Maibach and S. Kyranakis (2024). "A deep-learning strategy to identify cell types across species from high-density extracellular recordings." bioRxiv: 2024.2001.2030.577845.

Berke, J. D., M. Okatan, J. Skurski and H. B. Eichenbaum (2004). "Oscillatory entrainment of striatal neurons in freely moving rats." Neuron **43**(6): 883-896.

Bostan, A. C. and P. L. Strick (2018). "The basal ganglia and the cerebellum: nodes in an integrated network." Nature Reviews Neuroscience **19**(6): 338-350.

Caligiore, D., M. A. Arbib, R. C. Miall and G. Baldassarre (2019). "The super-learning hypothesis: Integrating learning processes across cortex, cerebellum and basal ganglia." Neuroscience & Biobehavioral Reviews **100**: 19-34.

Caligiore, D., G. Pezzulo, G. Baldassarre, A. C. Bostan, P. L. Strick, K. Doya, R. C. Helmich, M. Dirkx, J. Houk and H. Jörntell (2017). "Consensus paper: towards a systems-level view of cerebellar function: the interplay between cerebellum, basal ganglia, and cortex." The Cerebellum **16**: 203-229.

Chabrol, F. P., A. Blot and T. D. Mrsic-Flogel (2019). "Cerebellar contribution to preparatory activity in motor neocortex." Neuron **103**(3): 506-519. e504.

Chantranupong, L., C. C. Beron, J. A. Zimmer, M. J. Wen, W. Wang and B. L. Sabatini (2023). "Dopamine and glutamate regulate striatal acetylcholine in decision-making." Nature **621**(7979): 577-585.

Chen, C. H., R. Fremont, E. E. Arteaga-Bracho and K. Khodakhah (2014). "Short latency cerebellar modulation of the basal ganglia." Nature Neuroscience **17**(12): 1767-1775.

Cheron, G., M. Sausbier, U. Sausbier, W. Neuhuber, P. Ruth, B. Dan and L. Servais (2009). "BK channels control cerebellar Purkinje and Golgi cell rhythmicity in vivo." PLoS One **4**(11): e7991.

Chiken, S., P. Shashidharan and A. Nambu (2008). "Cortically evoked long-lasting inhibition of pallidal neurons in a transgenic mouse model of dystonia." Journal of Neuroscience **28**(51): 13967-

13977.
Courtemanche, R., J. C. Robinson and D. I. Aponte (2013). "Linking oscillations in cerebellar circuits." Frontiers in Neural Circuits **7**: 125.
Diedrichsen, J., R. B. Ivry and J. Pressing (2003). "Cerebellar and basal ganglia contributions to interval timing." Functional and neural mechanisms of interval timing: 457-481.
Doya, K. (1999). "What are the computations of the cerebellum, the basal ganglia and the cerebral cortex?" Neural networks **12**(7-8): 961-974.
Doya, K. (2000). "Complementary roles of basal ganglia and cerebellum in learning and motor control." Current opinion in neurobiology **10**(6): 732-739.
Foster, N. N., J. Barry, L. Korobkova, L. Garcia, L. Gao, M. Becerra, Y. Sherafat, B. Peng, X. Li and J.-H. Choi (2021). "The mouse cortico–basal ganglia–thalamic network." Nature **598**(7879): 188-194.
Fujimoto, K. and H. Kita (1992). "Responses of rat substantia nigra pars reticulata units to cortical stimulation." Neuroscience letters **142**(1): 105-109.
Gage, G. J., C. R. Stoetzner, A. B. Wiltschko and J. D. Berke (2010). "Selective activation of striatal fast-spiking interneurons during choice execution." Neuron **67**(3): 466-479.
Gambosi, B., F. J. Sheiban, M. Biasizzo, A. Antonietti, E. D'angelo, A. Mazzoni and A. Pedrocchi (2024). "A model with dopamine depletion in basal ganglia and cerebellum predicts changes in thalamocortical beta oscillations." International Journal of Neural Systems **2450045**: 21.
Gao, Z., C. Davis, A. M. Thomas, M. N. Economo, A. M. Abrego, K. Svoboda, C. I. De Zeeuw and N. Li (2018). "A cortico-cerebellar loop for motor planning." Nature **563**(7729): 113-116.
Gornati, S. V., C. B. Schäfer, O. H. E. Rooda, A. L. Nigg, C. I. De Zeeuw and F. E. Hoebeek (2018). "Differentiating cerebellar impact on thalamic nuclei." Cell Reports **23**(9): 2690-2704.
Grillner, S. (2021). "Evolution of the vertebrate motor system—from forebrain to spinal cord." Current Opinion in Neurobiology **71**: 11-18.
Halje, P., I. Brys, J. J. Mariman, C. Da Cunha, R. Fuentes and P. Petersson (2019). "Oscillations in cortico-basal ganglia circuits: implications for Parkinson's disease and other neurologic and psychiatric conditions." Journal of neurophysiology **122**(1): 203-231.
Harvey, R., R. Porter and J. Rawson (1979). "Discharges of intracerebellar nuclear cells in monkeys." The Journal of physiology **297**(1): 559-580.
Heffley, W. and C. Hull (2019). "Classical conditioning drives learned reward prediction signals in climbing fibers across the lateral cerebellum." elife **8**: e46764.
Hesslow, G., P. Svensson and M. Ivarsson (1999). "Learned movements elicited by direct stimulation of cerebellar mossy fiber afferents." Neuron **24**(1): 179-185.
Hintiryan, H., N. N. Foster, I. Bowman, M. Bay, M. Y. Song, L. Gou, S. Yamashita, M. S.

Bienkowski, B. Zingg and M. Zhu (2016). "The mouse cortico-striatal projectome." Nature Neuroscience **19**(8): 1100-1114.

Hira, R., N. Honkura, J. Noguchi, Y. Maruyama, G. J. Augustine, H. Kasai and M. Matsuzaki (2009). "Transcranial optogenetic stimulation for functional mapping of the motor cortex." Journal of Neuroscience Methods **179**(2): 258-263.

Hira, R., F. Ohkubo, K. Ozawa, Y. Isomura, K. Kitamura, M. Kano, H. Kasai and M. Matsuzaki (2013). "Spatiotemporal dynamics of functional clusters of neurons in the mouse motor cortex during a voluntary movement." Journal of Neuroscience **33**(4): 1377-1390.

Hira, R., F. Ohkubo, Y. R. Tanaka, Y. Masamizu, G. J. Augustine, H. Kasai and M. Matsuzaki (2013). "In vivo optogenetic tracing of functional corticocortical connections between motor forelimb areas." Frontiers in Neural Circuits **7**: 55.

Hira, R., S.-I. Terada, M. Kondo and M. Matsuzaki (2015). "Distinct functional modules for discrete and rhythmic forelimb movements in the mouse motor cortex." Journal of Neuroscience **35**(39): 13311-13322.

Hirano, T. (1990). "Depression and potentiation of the synaptic transmission between a granule cell and a Purkinje cell in rat cerebellar culture." Neuroscience letters **119**(2): 141-144.

Hoang, H., S. Tsutsumi, M. Matsuzaki, M. Kano, M. Kawato, K. Kitamura and K. Toyama (2023). "Dynamic organization of cerebellar climbing fiber response and synchrony in multiple functional components reduces dimensions for reinforcement learning." elife **12**: e86340.

Hoebeek, F. E., L. Witter, T. J. Ruigrok and C. I. De Zeeuw (2010). "Differential olivo-cerebellar cortical control of rebound activity in the cerebellar nuclei." Proceedings of the National Academy of Sciences **107**(18): 8410-8415.

Hooks, B. M., T. Mao, D. A. Gutnisky, N. Yamawaki, K. Svoboda and G. M. Shepherd (2013). "Organization of cortical and thalamic input to pyramidal neurons in mouse motor cortex." Journal of Neuroscience **33**(2): 748-760.

Houk, J. C., C. Bastianen, D. Fansler, A. Fishbach, D. Fraser, P. Reber, S. Roy and L. Simo (2007). "Action selection and refinement in subcortical loops through basal ganglia and cerebellum." Philosophical Transactions of the Royal Society B: Biological Sciences **362**(1485): 1573-1583.

Houk, J. C. and S. P. Wise (1995). "Distributed modular architectures linking basal ganglia, cerebellum, and cerebral cortex: their role in planning and controlling action." Cerebral cortex **5**(2): 95-110.

Ichinohe, N., F. Mori and K. Shoumura (2000). "A di-synaptic projection from the lateral cerebellar nucleus to the laterodorsal part of the striatum via the central lateral nucleus of the thalamus in the rat." Brain research **880**(1-2): 191-197.

Igarashi, J., Y. Isomura, K. Arai, R. Harukuni and T. Fukai (2013). "A $\theta-\gamma$ oscillation code for

neuronal coordination during motor behavior." Journal of Neuroscience **33**(47): 18515-18530.
Izhikevich, E. M. (2003). "Simple model of spiking neurons." IEEE Transactions on neural networks **14**(6): 1569-1572.
Izhikevich, E. M. (2007). Dynamical systems in neuroscience, MIT press.
Jelitai, M., P. Puggioni, T. Ishikawa, A. Rinaldi and I. Duguid (2016). "Dendritic excitation–inhibition balance shapes cerebellar output during motor behaviour." Nature Communications **7**(1): 13722.
Jeon, H., H. Lee, D.-H. Kwon, J. Kim, K. Tanaka-Yamamoto, J. S. Yook, L. Feng, H. R. Park, Y. H. Lim and Z.-H. Cho (2022). "Topographic connectivity and cellular profiling reveal detailed input pathways and functionally distinct cell types in the subthalamic nucleus." Cell Reports **38**(9).
Jun, J. J., N. A. Steinmetz, J. H. Siegle, D. J. Denman, M. Bauza, B. Barbarits, A. K. Lee, C. A. Anastassiou, A. Andrei and Ç. Aydın (2017). "Fully integrated silicon probes for high-density recording of neural activity." Nature **551**(7679): 232-236.
Kaneko, T. (2013). "Local connections of excitatory neurons in motor-associated cortical areas of the rat." Frontiers in Neural Circuits
7: 75.
Kawabata, M., S. Soma, A. Saiki-Ishikawa, S. Nonomura, J. Yoshida, A. Ríos, Y. Sakai and Y. Isomura (2020). "A spike analysis method for characterizing neurons based on phase locking and scaling to the interval between two behavioral events." Journal of neurophysiology **124**(6): 1923-1941.
Kebschull, J. M., E. B. Richman, N. Ringach, D. Friedmann, E. Albarran, S. S. Kolluru, R. C. Jones, W. E. Allen, Y. Wang and S. W. Cho (2020). "Cerebellar nuclei evolved by repeatedly duplicating a conserved cell-type set." Science **370**(6523): eabd5059.
Khanna, P. and J. M. Carmena (2015). "Neural oscillations: beta band activity across motor networks." Current opinion in neurobiology **32**: 60-67.
Kimura, R., A. Saiki, Y. Fujiwara-Tsukamoto, F. Ohkubo, K. Kitamura, M. Matsuzaki, Y. Sakai and Y. Isomura (2012). "Reinforcing operandum: rapid and reliable learning of skilled forelimb movements by head-fixed rodents." Journal of neurophysiology **108**(6): 1781-1792.
Kimura, R., A. Saiki, Y. Fujiwara - Tsukamoto, Y. Sakai and Y. Isomura (2017). "Large - scale analysis reveals populational contributions of cortical spike rate and synchrony to behavioural functions." The Journal of physiology **595**(1): 385-413.
Kitano, H., I. Tanibuchi and K. Jinnai (1998). "The distribution of neurons in the substantia nigra pars reticulata with input from the motor, premotor and prefrontal areas of the cerebral cortex in monkeys." Brain research **784**(1-2): 228-238.
Kostadinov, D. and M. Häusser (2022). "Reward signals in the cerebellum: origins, targets, and functional implications." Neuron.

Kuramoto, E., T. Furuta, K. C. Nakamura, T. Unzai, H. Hioki and T. Kaneko (2009). "Two types of thalamocortical projections from the motor thalamic nuclei of the rat: a single neuron-tracing study using viral vectors." Cerebral cortex **19**(9): 2065-2077.

Kuramoto, E., S. Ohno, T. Furuta, T. Unzai, Y. R. Tanaka, H. Hioki and T. Kaneko (2015). "Ventral medial nucleus neurons send thalamocortical afferents more widely and more preferentially to layer 1 than neurons of the ventral anterior–ventral lateral nuclear complex in the rat." Cerebral cortex **25**(1): 221-235.

Lake, B. M., T. D. Ullman, J. B. Tenenbaum and S. J. Gershman (2017). "Building machines that learn and think like people." Behavioral and brain sciences **40**: e253.

Ledergerber, D. and M. E. Larkum (2012). "The time window for generation of dendritic spikes by coincidence of action potentials and EPSPs is layer specific in somatosensory cortex." PLoS One **7**(3): e33146.

Lee, D., J. H. Hyun, K. Jung, P. Hannan and H.-B. Kwon (2017). "A calcium-and light-gated switch to induce gene expression in activated neurons." Nature Biotechnology **35**(9): 858-863.

Lee, J., W. Wang and B. L. Sabatini (2020). "Anatomically segregated basal ganglia pathways allow parallel behavioral modulation." Nature Neuroscience **23**(11): 1388-1398.

Leventhal, D. K., G. J. Gage, R. Schmidt, J. R. Pettibone, A. C. Case and J. D. Berke (2012). "Basal ganglia beta oscillations accompany cue utilization." Neuron **73**(3): 523-536.

Li, T., W. Le and J. Jankovic (2023). "Linking the cerebellum to Parkinson disease: an update." Nature Reviews Neurology **19**(11): 645-654.

Mallet, N., A. Pogosyan, L. F. Márton, J. P. Bolam, P. Brown and P. J. Magill (2008). "Parkinsonian beta oscillations in the external globus pallidus and their relationship with subthalamic nucleus activity." Journal of neuroscience **28**(52): 14245-14258.

Marlinski, V. and I. N. Beloozerova (2014). "Burst firing of neurons in the thalamic reticular nucleus during locomotion." Journal of neurophysiology **112**(1): 181-192.

Maurice, N., J.-M. Deniau, J. Glowinski and A.-M. Thierry (1999). "Relationships between the prefrontal cortex and the basal ganglia in the rat: physiology of the cortico-nigral circuits." Journal of Neuroscience **19**(11): 4674-4681.

Maurice, N., A.-M. Thierry, J. Glowinski and J.-M. Deniau (2003). "Spontaneous and evoked activity of substantia nigra pars reticulata neurons during high-frequency stimulation of the subthalamic nucleus." Journal of Neuroscience **23**(30): 9929-9936.

Middleton, S. J., C. Racca, M. O. Cunningham, R. D. Traub, H. Monyer, T. Knöpfel, I. S. Schofield, A. Jenkins and M. A. Whittington (2008). "High-frequency network oscillations in cerebellar cortex." Neuron **58**(5): 763-774.

Miller, B. R., A. G. Walker, A. S. Shah, S. J. Barton and G. V. Rebec (2008). "Dysregulated information processing by medium spiny neurons in striatum of freely behaving mouse models of

Huntington's disease." Journal of neurophysiology **100**(4): 2205-2216.
Mitani, K., M. Kawabata, Y. Isomura and Y. Sakai (2022). "Automated and parallelized spike collision tests to identify spike signal projections." iScience **25**(10).
Morén, J., J. Igarashi, O. Shouno, J. Yoshimoto and K. Doya (2019). "Dynamics of basal ganglia and thalamus in Parkinsonian tremor." Multiscale Models of Brain Disorders: 13-20.
Muddapu, V. R., A. Mandali, V. S. Chakravarthy and S. Ramaswamy (2019). "A computational model of loss of dopaminergic cells in Parkinson's disease due to glutamate-induced excitotoxicity." Frontiers in Neural Circuits
13: 11.
Murakami, T. C., T. Mano, S. Saikawa, S. A. Horiguchi, D. Shigeta, K. Baba, H. Sekiya, Y. Shimizu, K. F. Tanaka and H. Kiyonari (2018). "A three-dimensional single-cell-resolution whole-brain atlas using CUBIC-X expansion microscopy and tissue clearing." Nature Neuroscience **21**(4): 625-637.
Mushiake, H. and P. L. Strick (1993). "Preferential activity of dentate neurons during limb movements guided by vision." Journal of neurophysiology **70**(6): 2660-2664.
Muzzu, T., S. Mitolo, G. P. Gava and S. R. Schultz (2018). "Encoding of locomotion kinematics in the mouse cerebellum." PLoS One **13**(9): e0203900.
Nambu, A., S. Chiken, H. Sano, N. Hatanaka and J. A. Obeso (2023). "Dynamic Activity Model of Movement Disorders: The Fundamental Role of the Hyperdirect Pathway." Movement Disorders **38**(12): 2145-2150.
Nambu, A., H. Tokuno, I. Hamada, H. Kita, M. Imanishi, T. Akazawa, Y. Ikeuchi and N. Hasegawa (2000). "Excitatory cortical inputs to pallidal neurons via the subthalamic nucleus in the monkey." Journal of neurophysiology **84**(1): 289-300.
Nambu, A., H. Tokuno and M. Takada (2002). "Functional significance of the cortico–subthalamo–pallidal 'hyperdirect'pathway." Neuroscience Research **43**(2): 111-117.
O'Connor, D. H., S. P. Peron, D. Huber and K. Svoboda (2010). "Neural activity in barrel cortex underlying vibrissa-based object localization in mice." Neuron **67**(6): 1048-1061.
Ohmae, S., J. Kunimatsu and M. Tanaka (2017). "Cerebellar roles in self-timing for sub-and supra-second intervals." Journal of Neuroscience **37**(13): 3511-3522.
Penhune, V. B. and C. J. Steele (2012). "Parallel contributions of cerebellar, striatal and M1 mechanisms to motor sequence learning." Behavioural brain research **226**(2): 579-591.
Petter, E. A., N. A. Lusk, G. Hesslow and W. H. Meck (2016). "Interactive roles of the cerebellum and striatum in sub-second and supra-second timing: Support for an initiation, continuation, adjustment, and termination (ICAT) model of temporal processing." Neuroscience & Biobehavioral Reviews **71**: 739-755.
Pisano, T. J., Z. M. Dhanerawala, M. Kislin, D. Bakshinskaya, E. A. Engel, E. J. Hansen, A. T.

Hoag, J. Lee, N. L. de Oude and K. U. Venkataraju (2021). "Homologous organization of cerebellar pathways to sensory, motor, and associative forebrain." Cell Reports **36**(12): 109721.

Poirazi, P. and A. Papoutsi (2020). "Illuminating dendritic function with computational models." Nature Reviews Neuroscience **21**(6): 303-321.

Popa, D., M. Spolidoro, R. D. Proville, N. Guyon, L. Belliveau and C. Léna (2013). "Functional role of the cerebellum in gamma-band synchronization of the sensory and motor cortices." Journal of Neuroscience **33**(15): 6552-6556.

Popa, T., B. Velayudhan, C. Hubsch, S. Pradeep, E. Roze, M. Vidailhet, S. Meunier and A. Kishore (2013). "Cerebellar processing of sensory inputs primes motor cortex plasticity." Cerebral cortex **23**(2): 305-314.

Proville, R. D., M. Spolidoro, N. Guyon, G. P. Dugué, F. Selimi, P. Isope, D. Popa and C. Léna (2014). "Cerebellum involvement in cortical sensorimotor circuits for the control of voluntary movements." Nature Neuroscience **17**(9): 1233-1239.

Prsa, M., S. Dash, N. Catz, P. W. Dicke and P. Thier (2009). "Characteristics of responses of Golgi cells and mossy fibers to eye saccades and saccadic adaptation recorded from the posterior vermis of the cerebellum." Journal of Neuroscience **29**(1): 250-262.

Pugh, J. R. and I. M. Raman (2008). "Mechanisms of potentiation of mossy fiber EPSCs in the cerebellar nuclei by coincident synaptic excitation and inhibition." Journal of Neuroscience **28**(42): 10549-10560.

Saiki, A., Y. Sakai, R. Fukabori, S. Soma, J. Yoshida, M. Kawabata, H. Yawo, K. Kobayashi, M. Kimura and Y. Isomura (2018). "In vivo spiking dynamics of intra-and extratelencephalic projection neurons in rat motor cortex." Cerebral cortex **28**(3): 1024-1038.

Sano, H., S. Chiken, T. Hikida, K. Kobayashi and A. Nambu (2013). "Signals through the striatopallidal indirect pathway stop movements by phasic excitation in the substantia nigra." Journal of Neuroscience **33**(17): 7583-7594.

Schell, G. R. and P. L. Strick (1984). "The origin of thalamic inputs to the arcuate premotor and supplementary motor areas." Journal of Neuroscience **4**(2): 539-560.

Sedaghat-Nejad, E., M. A. Fakharian, J. Pi, P. Hage, Y. Kojima, R. Soetedjo, S. Ohmae, J. F. Medina and R. Shadmehr (2021). "P-sort: an open-source software for cerebellar neurophysiology." Journal of neurophysiology **126**(4): 1055-1075.

Sedaghat-Nejad, E., J. S. Pi, P. Hage, M. A. Fakharian and R. Shadmehr (2022). "Synchronous spiking of cerebellar Purkinje cells during control of movements." Proceedings of the National Academy of Sciences **119**(14): e2118954119.

Sendhilnathan, N., M. Semework, M. E. Goldberg and A. E. Ipata (2020). "Neural correlates of reinforcement learning in mid-lateral cerebellum." Neuron **106**(1): 188-198. e185.

Shadmehr, R. and J. W. Krakauer (2008). "A computational neuroanatomy for motor control."

Experimental brain research **185**: 359-381.
Shen, W., J. L. Plotkin, V. Francardo, W. K. D. Ko, Z. Xie, Q. Li, T. Fieblinger, J. Wess, R. R. Neubig and C. W. Lindsley (2015). "M4 muscarinic receptor signaling ameliorates striatal plasticity deficits in models of L-DOPA-induced dyskinesia." Neuron **88**(4): 762-773.
Shinoda, Y., Y. Sugiuchi, T. Futami and R. Izawa (1992). "Axon collaterals of mossy fibers from the pontine nucleus in the cerebellar dentate nucleus." Journal of neurophysiology **67**(3): 547-560.
Siegle, J. H., A. C. López, Y. A. Patel, K. Abramov, S. Ohayon and J. Voigts (2017). "Open Ephys: an open-source, plugin-based platform for multichannel electrophysiology." Journal of neural engineering **14**(4): 045003.
Spencer, R. M. and R. B. Ivry (2021). Cerebellum and timing. Handbook of the cerebellum and cerebellar disorders, Springer**:** 1359-1377.
Stein, E. and I. Bar-Gad (2013). "Beta oscillations in the cortico-basal ganglia loop during parkinsonism." Experimental Neurology **245**: 52-59.
Sugihara, I., H. Fujita, J. Na, P. N. Quy, B. Y. Li and D. Ikeda (2009). "Projection of reconstructed single Purkinje cell axons in relation to the cortical and nuclear aldolase C compartments of the rat cerebellum." Journal of Comparative Neurology **512**(2): 282-304.
Sugihara, I., H. Wu and Y. Shinoda (1996). "Morphology of axon collaterals of single climbing fibers in the deep cerebellar nuclei of the rat." Neuroscience letters **217**(1): 33-36.
Tanaka, M., M. Kameda and K.-i. Okada (2024). "Temporal Information Processing in the Cerebellum and Basal Ganglia." Neurobiology of Interval Timing: 95-116.
Tervo, D. G. R., B.-Y. Hwang, S. Viswanathan, T. Gaj, M. Lavzin, K. D. Ritola, S. Lindo, S. Michael, E. Kuleshova and D. Ojala (2016). "A designer AAV variant permits efficient retrograde access to projection neurons." Neuron **92**(2): 372-382.
Thach, W. T., H. Goodkin and J. Keating (1992). "The cerebellum and the adaptive coordination of movement." Annual review of neuroscience **15**(1): 403-442.
Thibeault, C. M. and N. Srinivasa (2013). "Using a hybrid neuron in physiologically inspired models of the basal ganglia." Frontiers in computational neuroscience **7**: 88.
Thoma, P., C. Bellebaum, B. Koch, M. Schwarz and I. Daum (2008). "The cerebellum is involved in reward-based reversal learning." The Cerebellum **7**: 433-443.
Tomita, H., E. Sugano, Y. Fukazawa, H. Isago, Y. Sugiyama, T. Hiroi, T. Ishizuka, H. Mushiake, M. Kato and M. Hirabayashi (2009). "Visual properties of transgenic rats harboring the channelrhodopsin-2 gene regulated by the thy-1.2 promoter." PloS one **4**(11): e7679.
Tsukahara, N., H. Korn and J. Stone (1968). "Pontine relay from cerebral cortex to cerebellar cortex and nucleus interpositus." Brain Research **10**(3): 448-453.
Ueki, Y., T. Mima, M. Ali Kotb, H. Sawada, H. Saiki, A. Ikeda, T. Begum, F. Reza, T. Nagamine and H. Fukuyama (2006). "Altered plasticity of the human motor cortex in Parkinson's disease."

Annals of neurology **59**(1): 60-71.
Urbain, N., P. A. Salin, P.-A. Libourel, J.-C. Comte, L. J. Gentet and C. C. Petersen (2015). "Whisking-related changes in neuronal firing and membrane potential dynamics in the somatosensory thalamus of awake mice." Cell Reports **13**(4): 647-656.
Van Dijck, G., M. M. Van Hulle, S. A. Heiney, P. M. Blazquez, H. Meng, D. E. Angelaki, A. Arenz, T. W. Margrie, A. Mostofi and S. Edgley (2013). "Probabilistic identification of cerebellar cortical neurones across species." PloS one **8**(3): e57669.
Van Kan, P. L., A. R. Gibson and J. C. Houk (1993). "Movement-related inputs to intermediate cerebellum of the monkey." Journal of neurophysiology **69**(1): 74-94.
Wagner, M. J., T. H. Kim, J. Kadmon, N. D. Nguyen, S. Ganguli, M. J. Schnitzer and L. Luo (2019). "Shared cortex-cerebellum dynamics in the execution and learning of a motor task." Cell **177**(3): 669-682. e624.
Wang, W., C. P. Wildes, T. Pattarabanjird, M. I. Sanchez, G. F. Glober, G. A. Matthews, K. M. Tye and A. Y. Ting (2017). "A light-and calcium-gated transcription factor for imaging and manipulating activated neurons." Nature Biotechnology **35**(9): 864-871.
Wang, Y., X. Yin, Z. Zhang, J. Li, W. Zhao and Z. V. Guo (2021). "A cortico-basal ganglia-thalamo-cortical channel underlying short-term memory." Neuron **109**(21): 3486-3499. e3487.
Wu, H. S., I. Sugihara and Y. Shinoda (1999). "Projection patterns of single mossy fibers originating from the lateral reticular nucleus in the rat cerebellar cortex and nuclei." Journal of Comparative Neurology **411**(1): 97-118.
Wu, X., G. A. Sarpong, J. Zhang and I. Sugihara (2023). "Divergent topographic projection of cerebral cortical areas to overlapping cerebellar lobules through distinct regions of the pontine nuclei." Heliyon **9**(4).
Yagishita, S., A. Hayashi-Takagi, G. C. Ellis-Davies, H. Urakubo, S. Ishii and H. Kasai (2014). "A critical time window for dopamine actions on the structural plasticity of dendritic spines." Science **345**(6204): 1616-1620.
Yamazaki, T. and W. Lennon (2019). "Revisiting a theory of cerebellar cortex." Neuroscience Research **148**: 1-8.
Yasoshima, Y., N. Kai, S. Yoshida, S. Shiosaka, Y. Koyama, Y. Kayama and K. Kobayashi (2005). "Subthalamic neurons coordinate basal ganglia function through differential neural pathways." Journal of Neuroscience **25**(34): 7743-7753.
Yoshida, J., M. Oñate, L. Khatami, J. Vera, F. Nadim and K. Khodakhah (2022). "Cerebellar contributions to the basal ganglia influence motor coordination, reward processing, and movement vigor." Journal of Neuroscience **42**(45): 8406-8415.
Yoshizawa, T., Y. Miyamura, Y. Ochi, R. Hira, M. Funahashi, Y. Sakai, Y. Cui and Y. Isomura (2023). "Working memory-based and-free reward prediction in a dual dopamine system in the

basal ganglia." bioRxiv: 2023.2003. 2006.531239.

Zhu, J., H. Hasanbegović, L. D. Liu, Z. Gao and N. Li (2023). "Activity map of a cortico-cerebellar loop underlying motor planning." Nature Neuroscience **26**(11): 1916-1928.